

**1 Evolution of the East Greenland Current from Fram**  
**2 Strait to Denmark Strait: Synoptic measurements**  
**3 from summer 2012**

L. Håvik<sup>1</sup>, R. S. Pickart<sup>2</sup>, K. Våge<sup>1</sup>, D. Torres<sup>2</sup>, A. M. Thurnherr<sup>3</sup>, A.  
Beszczynska-Möller<sup>4</sup>, W. Walczowski<sup>4</sup>, W.-J. von Appen<sup>5</sup>

---

Corresponding author: L. Håvik, Geophysical Institute and the Bjerknes Centre for Climate  
Research, University of Bergen, Norway. (lisbeth.havik@uib.no)

<sup>1</sup>Geophysical Institute, University of  
Bergen and Bjerknes Centre for Climate  
Research, Bergen, Norway

<sup>2</sup>Woods Hole Oceanographic Institution,  
Woods Hole, USA

<sup>3</sup>Lamont-Doherty Earth Observatory,  
Palisades, USA

<sup>4</sup>Institute of Oceanology Polish Academy  
of Sciences, Sopot, Poland

<sup>5</sup>Alfred Wegener Institute, Helmholtz  
Centre for Polar and Marine Research,  
Bremerhaven, Germany

**Key Points.**

- Two summer 2012 shipboard surveys document the evolution of the East Greenland Current (EGC) system from Fram Strait to Denmark Strait.
- The water mass and kinematic structure of the three distinct EGC branches are described using high-resolution measurements.
- Transports of freshwater and dense overflow water have been quantified for each branch.

4 **Abstract.** We present measurements from two shipboard surveys con-  
5 ducted in summer 2012 that sampled the rim current system around the Nordic  
6 Seas from Fram Strait to Denmark Strait. The data reveal that, along a por-  
7 tion of the western boundary of the Nordic Seas, the East Greenland Cur-  
8 rent (EGC) has three distinct components. In addition to the well-known shelf-  
9 break branch, there is an inshore branch on the continental shelf as well as  
10 a separate branch offshore of the shelfbreak. The inner branch contributes  
11 significantly to the overall freshwater transport of the rim current system,  
12 and the outer branch transports a substantial amount of Atlantic-origin Wa-  
13 ter equatorward. Supplementing our measurements with historical hydrographic  
14 data, we argue that the offshore branch is a direct recirculation of the west-  
15 ern branch of the West Spitsbergen Current in Fram Strait. The total trans-  
16 port of the shelfbreak EGC (the only branch sampled consistently in all of  
17 the sections) decreased towards Denmark Strait. The estimated average trans-  
18 port of dense overflow water ( $\sigma_\theta > 27.8 \text{ kg/m}^3$  and  $\Theta > 0 \text{ }^\circ\text{C}$ ) in the shelf-  
19 break EGC was  $2.8 \pm 0.7 \text{ Sv}$ , consistent with previous moored measurements.  
20 For the three sections that crossed the entire EGC system the freshwater flux,

<sup>21</sup> relative to a salinity of 34.8, ranged from  $127 \pm 13$  mSv to  $81 \pm 8$  mSv. The  
<sup>22</sup> hydrographic data reveal that, between Fram Strait and Denmark Strait, the  
<sup>23</sup> core of the Atlantic-origin Water in the shelfbreak EGC cools and freshens  
<sup>24</sup> but changes very little in density.

## 1. Introduction

25 The East Greenland Current (EGC) is a major pathway for transporting freshwater  
26 from the Arctic Ocean to the North Atlantic [*Haine et al.*, 2015], as well as an important  
27 supplier of dense overflow water to Denmark Strait [*Strass et al.*, 1993; *Jochumsen et al.*,  
28 2012; *Harden et al.*, 2016]. Numerous studies have focused on the EGC in both Fram and  
29 Denmark Straits; however, the region in between has only been sparsely observed and  
30 hence the along-stream evolution of the current remains largely unexplored. As water  
31 exits the Arctic Ocean in the EGC through Fram Strait, it is supplemented by a cross-  
32 strait flux of warm and saline water emanating from the West Spitsbergen Current (WSC).  
33 These recirculating waters, which originate from the North Atlantic via the Norwegian  
34 Atlantic Current, enhance the annual mean volume transport of the EGC by at least 3 Sv,  
35 resulting in a total southward transport of 8.7 Sv at 78°50'N [*de Steur et al.*, 2014].

36 Downstream of Fram Strait, *Woodgate et al.* [1999] estimated the transport of the  
37 EGC from a mooring array deployed across the current at 75°N in 1994-1995. They  
38 found a throughput of  $8 \pm 1$  Sv, with no apparent seasonal signal. Farther south the  
39 volume transport of the current gradually decreases as water is diverted into the Jan  
40 Mayen Current [*Bourke et al.*, 1992] and the East Icelandic Current [*Macrander et al.*,  
41 2014] (Fig. 1). At the northern end of the Blosseville Basin the EGC bifurcates into two  
42 distinct branches: the shelfbreak EGC and the separated EGC. The former continues  
43 southward along the east Greenland shelfbreak, while the latter veers offshore and follows  
44 the base of the Iceland slope toward Denmark Strait [*Våge et al.*, 2013; *Harden et al.*,  
45 2016]. While the Jan Mayen and East Icelandic Currents flow into the interior of the

46 Greenland and Iceland Seas, respectively, the two branches of the EGC in the Blosseville  
47 Basin pass through Denmark Strait into the North Atlantic.

48 The export of dense overflow water from the Nordic Seas contributes to the deep limb  
49 of the Atlantic Meridional Overturning Circulation. Approximately half of this export  
50 takes place through Denmark Strait [*Hansen and Østerhus, 2000*], and more than two-  
51 thirds of that is associated with the EGC [*Harden et al., 2016*]. Hence, knowledge of the  
52 upstream evolution of the current is essential for understanding the processes that dictate  
53 the supply of dense overflow water to Denmark Strait. *Mauritzen* [1996] concluded that  
54 Atlantic Water modified along the perimeter of the Nordic Seas is the main contributor to  
55 the overflow water that enters the strait via the EGC. This warm-to-cold conversion takes  
56 place predominantly in the northeastern Nordic Seas, due to strong buoyancy forcing in  
57 that region [*Isachsen et al., 2007*]. On the other hand, *Strass et al.* [1993] argued that  
58 as much as half of the transport of dense overflow water through Denmark Strait can be  
59 formed by isopycnal mixing between the recirculated Atlantic-origin Water in the EGC  
60 and the interior waters of the Greenland Sea. However, this mechanism may exhibit large  
61 interannual variability and the transport estimates are based on particular assumptions  
62 about the structure of the velocity field.

63 The surface layer of the EGC has a high freshwater content due to its origin in the  
64 Arctic Ocean, as well as from seasonal ice melt in the Nordic Seas and Fram Strait  
65 [*Rudels et al., 2002*]. The composition of the freshwater has been examined both from  
66 transects across the EGC from Fram Strait to Denmark Strait [*de Steur et al., 2015*] and  
67 within Fram Strait itself from a combination of in situ measurements and an inverse model  
68 [*Rabe et al., 2013*]. However, due to a lack of velocity measurements, only a few estimates

69 of the EGC freshwater transport are available. *Holfort and Meincke* [2005] obtained a  
70 total (liquid and solid) freshwater transport of 40-55 mSv relative to a reference salinity  
71 of 34.9 from moorings deployed on the east Greenland shelf close to 74°N in 2001-2002.  
72 Using data from the 2002 RV Oden expedition, *Nilsson et al.* [2008] estimated an average  
73 freshwater flux of 60 mSv. They concluded that the freshwater was largely conserved in  
74 the EGC as it progressed from north of Fram Strait to south of Denmark Strait. A decade  
75 of moored observations in Fram Strait indicated that the EGC has a relatively constant  
76 annual mean liquid freshwater flux of 40 mSv [*de Steur et al.*, 2009]. Based on model  
77 results, *de Steur et al.* [2009] estimated an additional flux of freshwater on the Greenland  
78 shelf of 26 mSv – emphasizing that the sparse measurements on the wide shelf could lead  
79 to an underestimate of the flux. *Rabe et al.* [2009] concluded that a considerable part of  
80 the freshwater transport through Fram Strait took place on the shelf rather than along  
81 the slope, and estimated a mean transport from three summer sections of  $80 \pm 6$  mSv. An  
82 overview of the freshwater fluxes east of Greenland can be found in *Holfort et al.* [2008].

83 To date there have been relatively few high-resolution transects – especially with velocity  
84 measurements – across the EGC in the Nordic Seas, partly because of the presence of pack  
85 ice (see Fig. 4 in *Seidov et al.* [2015] for an overview of the historical data). *Seidov et al.*  
86 [2015] calculated climatologies of temperature and salinity on a  $0.25^\circ \times 0.25^\circ$  grid for  
87 the Nordic Seas to investigate decadal variability of hydrographic properties. However,  
88 it is clear that variability on short time and space scales cannot be assessed from such  
89 a climatological data assembly. Numerical models are very powerful tools for evaluating  
90 ocean variability, water mass transformation, and current pathways. Most models capture  
91 the southward transport along the coast of east Greenland, but, in order to resolve the

92 more subtle features, fairly high resolution is required. The model employed by *Bacon*  
93 *et al.* [2014] of the East Greenland Coastal Current (EGCC) south of Denmark Strait has  
94 a resolution of  $1/12^\circ$ , corresponding to around 5 km. They conclude that this is sufficient  
95 to resolve the EGCC which typically has a width between 15 and 20 km. Unfortunately  
96 their analysis only covers the east Greenland shelf south of Denmark Strait. North of  
97 Denmark Strait, *Köhl et al.* [2007] presented results from a model with a resolution of  
98  $1/10^\circ$ . Their focus is on the water masses contributing to the Denmark Strait Overflow  
99 Water, and no detailed description of the EGC is provided. As pointed out in *Bacon et al.*  
100 [2014], it is important to validate the model output against observations, in particular in  
101 this region where there are still many uncertain aspects regarding the circulation and  
102 water masses.

103 Only two previous cruises have sampled the EGC from Fram Strait to Denmark Strait  
104 as part of a single survey. In fall 1998 five sections across the EGC were measured  
105 by RV Polarstern. A detailed description of the hydrographic properties of the water  
106 masses that constitute the EGC is presented in *Rudels et al.* [2002], but no velocity  
107 measurements or transport estimates are discussed. In 2002, RV Oden traversed the East  
108 Greenland Current five times within the same region. Their focus was on the along-  
109 stream changes in the water mass characteristics based on hydrographic and chemical  
110 measurements [*Rudels et al.*, 2005; *Jeansson et al.*, 2008]. The velocity measurements  
111 obtained were primarily used to calculate freshwater fluxes [*Nilsson et al.*, 2008]. As such,  
112 no previous studies have robustly characterized the kinematic structure of the current nor  
113 estimated its along-stream changes in volume transport.

114 In this study we use a set of 8 high-resolution shipboard transects across the EGC  
115 occupied during summer 2012 from Fram Strait to Denmark Strait to investigate the  
116 along-stream evolution of the current, its velocity and water mass structure, and the  
117 transport of both freshwater and dense overflow water. To address the importance of  
118 the recirculating Atlantic-origin Water in Fram Strait to the EGC system, we use three  
119 sections of the WSC occupied during the same summer, as well as historical data in the  
120 strait itself. We demonstrate that the EGC is in fact a system of distinct branches, from  
121 the inner shelf to the outer slope, which undergo significant modification as they progress  
122 equatorward in the Nordic Seas.

## 2. Data and Methods

### 2.1. East Greenland Current

123 The EGC data set was collected on a survey carried out on the RRS James Clark  
124 Ross, which began in Denmark Strait in late July and ended in Fram Strait in late  
125 August 2012. Here we use 8 transects across the east Greenland shelf and slope (Fig. 1),  
126 with particular emphasis on section 10 in the southern Fram Strait, section 6 along the  
127 Jan Mayen Fracture Zone, and section 3 in the Blosseville Basin. These three sections  
128 are representative of the general hydrographic structure and kinematic features of the  
129 current system between Fram Strait and Denmark Strait. The distance between stations  
130 was typically 5-7 km, which is close to the Rossby radius of deformation in this region  
131 (approximately 5 km [*Nurser and Bacon, 2014*]).

132 A Sea-Bird 911+ conductivity-temperature-depth (CTD) instrument was mounted on  
133 a rosette containing twelve 10-liter Niskin bottles. Downcast profiles of temperature and  
134 salinity were averaged into 2 db bins, from which other variables were computed. The



135 accuracy of the CTD measurements was 0.3 db for pressure, 0.001 °C for temperature,  
136 and 0.002 for salinity (see *Våge et al.* [2013]). Velocity profiles were obtained at each site  
137 using a lowered acoustic Doppler current profiler (LADCP) system attached to the rosette,  
138 consisting of upward- and downward-facing RDI 300-kHz instruments. An updated version  
139 of the barotropic tidal model of *Egbert and Erofeeva* [2002], with a resolution of  $1/60^\circ$ , was  
140 used to detide the velocity data before they were rotated into along- and across-section  
141 components. The uncertainty in the tidal model is mostly related to its representation  
142 of the bathymetry. We estimate this error by comparing the model bathymetry to the  
143 measured bathymetry and scale this ratio by the tidal velocity. The tidal currents were  
144 strongest in the southern sections, particularly in section 2, where this resulted in an error  
145 of approximately 2 cm/s. Conservatively, we use this value for all sections although the  
146 model likely performs slightly better farther north.

147 Vertical sections of potential temperature, salinity, and velocity were constructed by  
148 interpolation onto a regular grid with a resolution of 10 m in the vertical and 3 km  
149 in the horizontal using a Laplacian-spline routine [*Pickart and Smethie*, 1998]. Absolute  
150 geostrophic velocity sections were calculated by referencing the geostrophic shear obtained  
151 from the gridded hydrography using similarly gridded detided velocities from the LADCP.  
152 The mean values of the relative and directly measured velocities were matched between  
153 50 m and the bottom for each gridded profile. Velocity error estimates were calculated  
154 following the method outlined in *Sutherland* [2008]. This method combines the errors from  
155 the detiding routine and ageostrophic effects such as baroclinic tides in a root-sum-square  
156 fashion. The error is reduced by the square root of the number of station pairs covering  
157 the current branch in question (equivalent to number of degrees of freedom). With this

158 method the error increases if the station spacing is large and the width of the current is  
 159 narrow, i.e. where the current is resolved by only a few stations. This resulted in typical  
 160 velocity errors of 1-3 cm/s.

161 The freshwater transport (FWT) for each section was calculated as

$$FWT = \int_E^W \int_{z=S_{ref}}^{z=0} AGV(x, z) \cdot \frac{S_{ref} - S(z)}{S_{ref}} dz dx; \quad (1)$$

162 where  $S_{ref}$  is the reference salinity of 34.8 (same as that used in *Våge et al. [2013]*),  
 163 AGV is the absolute geostrophic velocity, and E and W correspond to the eastern and  
 164 western ends of each gridded section. Error estimates for volume transport were obtained  
 165 by multiplying the error velocity by the area of the current. For the FWT this number  
 166 was reduced by the amount of freshwater present, expressed by the fraction in Eq. 1.

## 2.2. West Spitsbergen Current and Fram Strait

167 We also use data from a hydrographic/velocity survey conducted in summer 2012 by  
 168 the Institute of Oceanology, Polish Academy of Sciences (IOPAN) in the northeastern  
 169 part of the boundary current system of the Nordic Seas. In particular, three sections are  
 170 used that were occupied in and south of Fram Strait (see Fig. 1). The cruise took place  
 171 roughly one month earlier than the EGC survey. A similar set-up was used consisting of  
 172 a Sea-Bird 911+ CTD mounted on a 12-bottle rosette with 12-liter bottles (only 9 bottles  
 173 were used in order to make room for the LADCP). The temperature and pressure sensors  
 174 underwent pre- and post-cruise laboratory calibrations, and the conductivity sensors were  
 175 calibrated using the in-situ water sample data. The errors were estimated as 1 db for  
 176 pressure, 0.001 °C for temperature, and 0.002 for salinity.

177 A single downward-facing RDI 300 kHz LADCP was used to obtain vertical profiles of  
178 horizontal velocity. This resulted in limited data coverage in the upper 50 m, and, due to  
179 large instrument tilts during the casts, there were some instances of data gaps at depth.  
180 Nonetheless, the overall data quality was good, and the velocity profiles were detided using  
181 the same model employed for the EGC profiles. The CTD data from the IOPAN survey  
182 were gridded, and the geostrophic velocities referenced, in the same fashion as the data  
183 from the EGC, except with a horizontal grid spacing of 5 km due to the coarser station  
184 spacing. Note that sections E7 and 10 in the southern Fram Strait were approximately  
185 along the same latitude (Fig. 1), and the combination of these resulted in a complete  
186 transect across the strait.

187 To complement our analysis of the boundary current system of the Nordic Seas we  
188 collected historical CTD data from meridional sections in Fram Strait obtained during  
189 summers 1997, 1998, 1999, 2002, 2003 and 2004 from the PANGAEA database [*Hansen,*  
190 *2006a, b, c; Schauer and Budéus, 2010; Schauer, 2010; Schauer and Rohardt, 2010*]. The  
191 hydrographic variables for each of the meridional sections were gridded using the same  
192 interpolation scheme with a resolution of 0.1 degree latitude and 10 m in the vertical.  
193 Due to the lack of direct velocity measurements we calculated geostrophic velocities from  
194 the hydrography relative to a level of no motion at 1000 m for these sections.

### 3. Hydrographic Structure of the East Greenland Current

195 In every crossing of the east Greenland shelf and slope, the hydrography of the EGC  
196 had a three-layered structure. This is illustrated nicely by the temperature and salinity  
197 fields from section 10 (Fram Strait), section 6 (Jan Mayen Fracture Zone), and section 3  
198 (Blosseville Basin) (first two panels of Figs. 2, 3, and 4, respectively). The surface layer

199 consists of fresh Polar Surface Water (PSW) extending all the way across most of the  
200 sections. In the upper few meters this layer is warmer due to summer insolation, but the  
201 temperature rapidly decreases below that. The outermost station on section 9 and the  
202 stations offshore of approximately  $x = 85$  km on section 10 were the only ones without this  
203 fresh surface layer. On the shelf the surface layer is roughly 150-200 m thick, becoming as  
204 thin as 50 m offshore. This results in a pronounced upward tilt of the isopycnals towards  
205 the east.

206 Immediately below the PSW is the warmer and saltier Atlantic-origin Water. This is  
207 broadly defined as all intermediate waters with a temperature above  $0\text{ }^{\circ}\text{C}$  [*Våge et al.*,  
208 2011]. At the two northernmost sections the Atlantic-origin Water could be separated  
209 into two distinct components: the warm and saline Atlantic Water originating directly  
210 from the WSC in Fram Strait, and the colder and less saline Arctic Atlantic Water that  
211 is generally situated deeper on the east Greenland slope [*Rudels et al.*, 2002]. The latter  
212 enters the Arctic Ocean via the WSC or through the Barents Sea, and is modified while  
213 flowing through the Arctic Ocean before exiting Fram Strait in the EGC. South of section 9  
214 these two water masses were difficult to distinguish. *Rudels et al.* [2005] referred to the  
215 combination of the two Atlantic-origin water masses as Return Atlantic Water but we  
216 will refer to the mixture simply as Atlantic-origin Water. The Atlantic-origin layer is  
217 characterized by an intermediate maximum in temperature and salinity, and is typically  
218 500-700 m thick. Below this, i.e. below the deep  $0\text{ }^{\circ}\text{C}$  isotherm, resides the colder and less  
219 saline lower-intermediate layer.

220 The water masses at the offshore ends of the transects differed north and south of the  
221 Jan Mayen Fracture Zone. In the Greenland Sea, the Atlantic-origin Water was present

222 across the entire sections with a clear intermediate salinity and temperature maximum.  
223 From section 6 and southward, however, the offshore water mass was less saline and  
224 colder, quite distinct from the Atlantic-origin Water (note the fresher water between 50  
225 and 400 m at the outer two stations in Fig. 3b). We generically refer to the waters  
226 offshore of the Atlantic-origin Water as ambient water, even though the characteristics  
227 differed from section to section.

228 In addition to distinguishing the water masses in terms of their potential tempera-  
229 ture/salinity ( $\theta/S$ ) characteristics, we divided the surface and intermediate waters by the  
230  $27.7 \text{ kg/m}^3$  isopycnal following *Rudels et al.* [2002]. This is a broader definition than the  
231 above separation into PSW and intermediate Atlantic-origin Water, which was useful off-  
232 shore of the EGC system where the  $\theta/S$  properties did not allow for an easy classification  
233 of the water masses. Within the EGC, where the boundary between the PSW and the  
234 Atlantic-origin Water was sharp, the density definition to a large degree coincides with  
235 the  $\theta/S$  definition (see for example Fig. 3b). *Rudels et al.* [2002] further separated the  
236 intermediate layer from the deep waters by the  $\sigma_{0.5} = 30.444 \text{ kg/m}^3$  isopycnal. However,  
237 due to the limited sampling at depth in the northernmost sections, we focus the analysis  
238 on the intermediate waters down to the deep  $0 \text{ }^\circ\text{C}$  isotherm.

#### 4. Velocity Structure of the East Greenland Current

239 As an overview of the current structure adjacent to Greenland, we show the depth-  
240 integrated LADCP vectors from the surface to 500 m for each station (Fig. 5). At the  
241 locations where the bottom depth was shallower than 500 m the integration was made to  
242 the bottom. In general, the highest velocities in each section are found in the vicinity of  
243 the shelfbreak and upper continental slope. However, note that there is strong flow on the

244 inner shelf for those crossings that extended close to the Greenland coast (sections 2, 3,  
245 and 6). In addition, there are instances of large velocities well seaward of the shelfbreak  
246 (e.g. sections 2 and 9).

247 Inspection of the vertical sections of absolute geostrophic velocity reveals that the EGC  
248 can be considered a system of distinct branches. North of  $71^{\circ}\text{N}$  there is an offshore  
249 velocity core that we refer to as the outer EGC. This was observed in sections 10, 9,  
250 and 6 (see the bottom panels of Figs. 2 and 3). In section 10 it was associated with a  
251 pronounced thinning of the Atlantic-origin layer, while at sections 9 and 6 it coincided  
252 with the transition from the Atlantic-origin Water to the ambient water farther offshore.  
253 In all cases the current was supported by a density front (upward-sloping isopycnals in  
254 the offshore direction). There is also a well-defined jet on the shelf that was present on  
255 the transects that extended close to the Greenland coast (sections 6, 3, and 2; see Figs. 3  
256 and 4). This is termed the PSW Jet and is also associated with a density front, in this  
257 case due to a thinning of the cold and fresh surface layer. The presence of both the outer  
258 EGC and the PSW Jet was mentioned by *Nilsson et al.* [2008]. However, they did not  
259 elaborate on the importance or implications of these separate components, and made no  
260 quantitative estimates of their transports. Finally, there is enhanced equatorward flow  
261 in the vicinity of the shelfbreak on all of the transects. Keeping with the nomenclature  
262 introduced by *Våge et al.* [2013], this jet is referred to as the shelfbreak EGC. Immediately  
263 offshore of that the flow was weaker and at times reversed.

264 In the southern part of the domain, specifically in sections 2 and 3 within the Blosseville  
265 Basin, the separated EGC was readily identifiable as a surface-intensified current centered  
266 over the base of the Iceland slope. These various kinematic components of the boundary

267 current system were manifest differently from section to section (see for example the  
268 bottom panels of Figs. 2, 3, and 4). In addition, mesoscale eddies were sampled on some  
269 of the sections. Due to this variability, an objective measure for delimiting each of the  
270 features was difficult to obtain; hence they were subjectively distinguished using their  
271 hydrographic and velocity structure as detailed below. The distinct components of the  
272 EGC current system are labeled at the top of the velocity sections in Figs. 2, 3, and 4,  
273 and will be discussed separately in the following sections.

#### 4.1. The Shelfbreak EGC

274 The shelfbreak EGC was the most prominent component of the boundary current sys-  
275 tem. It was characterized by strong surface-intensified flow close to the shelfbreak with  
276 a depth-dependent deep extension. The center of the current was objectively identified  
277 as the location with the highest mean absolute geostrophic velocity over the top 150 m  
278 across the section. In all cases this was associated with a density front, characterized  
279 by a steep shoaling of the  $27.5 \text{ kg/m}^3$  isopycnal. It also generally corresponded to the  
280 hydrographic front between the PSW and the Atlantic-origin Water. The bounding limits  
281 of the shelfbreak EGC were typically chosen as the locations where the mean velocity over  
282 the upper 150 m was reduced to 20 % of the core value. This worked as a guideline, but  
283 in several instances we subjectively chose the boundaries by combining the characteris-  
284 tic hydrography of the shelfbreak EGC and the steep slope of the  $27.5 \text{ kg/m}^3$  isopycnal  
285 towards the east. The resulting borders of the current are marked by the black vertical  
286 lines in the velocity sections of Figs. 2, 3, and 4.

287 The width and strength of the shelfbreak EGC varied considerably from section to  
288 section (Fig. 6). The core speed ranged between 0.2 and 0.4 m/s, but showed no clear

289 trend from north to south. The width of the current varied from a maximum value of  
290 80 km at section 9 to only 22 km at section 4, with indication of an overall decrease as the  
291 current progressed from Fram Strait to Denmark Strait. For the most part the width and  
292 the strength varied out of phase with each other: a strong current core coincided with a  
293 narrow jet and vice versa.

#### 4.2. The Polar Surface Water Jet

294 At each of the transects that sampled close to the east Greenland coast a surface-  
295 intensified jet was present within the PSW layer, onshore of – and distinct from – the  
296 shelfbreak EGC. This PSW Jet was completely bracketed on sections 6, 3, and 2, and  
297 partly sampled on sections 8 and 4 (the latter two sections did not extend sufficiently far  
298 onshore to fully sample the feature). The jet carried mostly PSW, but a weak extension to  
299 the bottom also resulted in transport of some Atlantic-origin Water that had penetrated  
300 onto the shelf. The velocity of the current was slightly lower than the shelfbreak EGC,  
301 with a peak value close to 0.2 m/s in section 3 (the core was defined in similiar fashion  
302 to the shelfbreak EGC). Due to the low salinity of the PSW, this branch of the current  
303 system is very important for the freshwater transport (discussed below in Section 5.2).

304 South of Denmark Strait the East Greenland Coastal Current (EGCC) is a well-  
305 established feature [*Bacon et al.*, 2002; *Sutherland and Pickart*, 2008]. The PSW Jet  
306 shares some similarities with this current, such as the proximity to the coast and its hy-  
307 drographic structure, although the velocities within the PSW Jet were generally weaker  
308 than those of the EGCC [*Sutherland and Pickart*, 2008]. The volume transports of the  
309 PSW Jet in the sections that fully resolved it were in the range of  $0.54 \pm 0.28$  Sv to  
310  $0.83 \pm 0.27$  Sv. These transports are comparable to the values obtained by *Sutherland*



311 *and Pickart* [2008] for the EGCC, ranging from 0.6-1.4 Sv, as well as the estimate by  
312 *Bacon et al.* [2002] of 1 Sv. *Bacon et al.* [2008] suggested that the EGCC could also be  
313 present north of Denmark Strait. They calculated the volume transport of the coastal  
314 current observed by *Nilsson et al.* [2008] close to 72°N to be 0.77 Sv.

315 *Bacon et al.* [2002] described the formation of the EGCC as a result of meltwater  
316 runoff from Greenland leading to a strengthening of the cross-shelf salinity gradient. This  
317 process is likely seasonal, with strongest current velocities in summer when the amount  
318 of meltwater is largest. By contrast, *Sutherland and Pickart* [2008] suggested that the  
319 EGCC is formed by a bifurcation of the shelfbreak EGC south of Denmark Strait due to  
320 bathymetric steering by the Kangerdlugssuaq Trough. If the EGCC is in fact the result  
321 of branching of the EGC south of Denmark Strait, then the PSW Jet is obviously not the  
322 same feature as the EGCC. On the other hand, if the EGCC stems from meltwater runoff  
323 as proposed by *Bacon et al.* [2002] then there is no geographical reason why it cannot  
324 also be present north of Denmark Strait. However, the presence of a coastal current  
325 during spring presented in *Nilsson et al.* [2008] shows that this feature is not restricted to  
326 summer. At present it remains unclear whether the PSW Jet is connected to the EGCC  
327 and what mechanism is responsible for generating this branch.

### 4.3. The outer EGC

328 Offshore of the shelfbreak EGC, at sections 6, 9, and 10, we observed a distinct branch  
329 advecting Atlantic-origin Water equatorward (see bottom panels of Figs. 2 and 3). As  
330 is the case with the shelfbreak EGC, this outer branch of the EGC is associated with a  
331 density front (i.e. shoaling isopycnals offshore), although the baroclinic shear is weaker.  
332 At section 8 this current branch was not observed and the current velocities offshore of

333 the shelfbreak current were weak (Fig. 5). This could be the result of a meandering of this  
334 outer branch offshore of our section, or synoptic variability masking its presence. Using  
335 data from a year-long deployment of moorings in the EGC, stretching from the slope  
336 toward the interior Greenland Sea at 75°N, *Woodgate et al.* [1999] found that the current  
337 had two independent cores: one at the shelfbreak and one at the base of the continental  
338 slope. This was not a persistent feature in their timeseries, and at times the two cores  
339 appeared to merge.

340 In order to investigate the relationship of the outer EGC to the boundary current sys-  
341 tem in the eastern Nordic Seas – specifically to the Atlantic Water approaching Fram  
342 Strait - we considered sections E7, E6, and E4 from the IOPAN survey (see Figs. 1 and 7b  
343 for the IOPAN section locations). In the eastern sections an analogous offshore current  
344 core, seaward of the eastern WSC, was present (not shown). This is the western branch  
345 of the WSC which constitutes the northward extension of the Norwegian Atlantic Frontal  
346 Current (NwAFC) [*Orvik and Niiler, 2002; Walczowski, 2013*]. The western branch ad-  
347 vects Atlantic Water towards Fram Strait along the slope of the Knipovich Ridge (Fig.  
348 1). To investigate a possible link between the two outer current cores, we constructed a  
349 composite summer section along the 0°E meridian in Fram Strait using the historical CTD  
350 data described in Section 2.2 (Figs. 1 and 7b). The composite section reveals the presence  
351 of a core of warm and saline Atlantic-origin Water located between 78°N and 79°N (Fig.  
352 8a,b). Notably, the hydrographic properties of the Atlantic Water flowing northward to-  
353 wards Fram Strait in the western WSC closely match both the warm and salty water in  
354 the composite section as well as the Atlantic-origin Water flowing southward in the outer  
355 core of the EGC (Fig. 7a, where for clarity we show only the profiles from 2003 in Fram

356 Strait). This suggests that the outer core of the EGC is the continuation of the western  
357 branch of the WSC, in accordance with the notion of a direct recirculation of Atlantic  
358 Water in Fram Strait north of sections E7 and 10 (e.g. *Quadfasel et al.* [1987]; *Manley*  
359 [1995]; *Fahrbach et al.* [2001]; *Marnela et al.* [2013]).

360 Unfortunately there are no corresponding velocity data to the historical hydrographic  
361 data, but the baroclinic shear relative to 1000 m is consistent with a region of surface-  
362 intensified westward flow associated with the hydrographic front on the northern side of  
363 the warm, salty core (Fig. 8c). This provides further evidence that the western branch  
364 of the WSC retroflects in Fram Strait and that this is the outer branch of the EGC  
365 that we sample farther downstream. Progressing along this recirculating branch, the  
366 transport of Atlantic-origin Water steadily decreases (Fig. 7c). Note that the transports  
367 were estimated perpendicular to the sections, and hence the actual transport might be  
368 larger depending on the direction of the flow. We have made no attempt to estimate the  
369 transport across the composite meridional section because of the lack of direct velocity  
370 information there. There is a particularly large drop in transport of the western branch of  
371 the WSC from section E4 to section E6, which may be influenced by a couple of factors.  
372 Firstly, *Walczowski and Piechura* [2007] found that part of the NwAFC is diverted offshore  
373 well south of Fram Strait. While their data suggest that this happens south of section E4,  
374 it could be a spatially or temporally varying process and our results may be a reflection  
375 of this. Secondly, a mesoscale eddy was located at the offshore end of section E4 which  
376 made it difficult to precisely estimate the transport of the western branch at that location;  
377 this is reflected by the large error bar corresponding to the E4 transport value (Fig. 7c).  
378 Nonetheless it is clear that, despite the synoptic nature of the two shipboard surveys,

379 there is a systematic decrease in transport of the outer core of Atlantic-origin Water as it  
380 flows along the perimeter of the Nordic Seas toward Denmark Strait.

381 The notion of a direct recirculation across Fram Strait has been discussed in a number of  
382 previous studies, and this flow is referred to as the Return Atlantic Current (e.g. *Paquette*  
383 *et al.* [1985]; *Quadfasel et al.* [1987]). *Manley* [1995] found that the recirculation took  
384 place south of 79°N. *Bourke et al.* [1988] estimated the transport from continuity to be  
385 0.8 Sv, which is lower than our value of 1.6 Sv in section 10. Also, based on conservation  
386 constraints, *Marnela et al.* [2013] estimated the recirculation of Atlantic Water to be  
387 about 2 Sv. A mooring array has monitored the flow through Fram Strait since 1997  
388 (e.g. *de Steur et al.* [2009]; *Beszczyńska-Möller et al.* [2012]). In 2002 the moorings in the  
389 western part of the strait were moved from 79°N to 78°50'N, resulting in an increase in  
390 the volume transport of the EGC of about 3 Sv. This suggests that a recirculation of  
391 Atlantic-origin Water of this magnitude takes place south of 79°N [*de Steur et al.*, 2014].  
392 It should be noted that this is the total change in the volume transport of the EGC, and  
393 not directly comparable to the recirculation resulting in the outer EGC. Using a high-  
394 resolution numerical model, *Aksenov et al.* [2010] referred to the recirculation in Fram  
395 Strait as the Knipovich Branch, and calculated a volume transport of 1.2 Sv. This was  
396 supported by *Hattermann et al.* [2016], who found a similar recirculation in the southern  
397 Fram Strait which they linked to the cyclonic gyre circulation in the Greenland Sea.  
398 However, our measurements indicate that the outer EGC branch is also present south of  
399 the Greenland Sea gyre (section 6). In the early studies that first introduced the term  
400 Return Atlantic Current, it was depicted as a flow that merged with the shelfbreak EGC

401 beneath the PSW layer. We have shown instead that these two features exist side-by-side  
402 in the Greenland Sea, at least as far south as the Jan Mayen Fracture Zone.

#### 4.4. The Separated EGC and eddies in the Blosseville Basin

403 The separated branch of the EGC in the Blosseville Basin, first identified by *Våge*  
404 *et al.* [2013], was evident in sections 2 and 3 (we note that *Våge et al.* [2013] included  
405 section 2 in their study). In section 3 this branch was situated close to  $x = 165$  km,  
406 identifiable as a distinct surface-intensified current with a deep extension to the bottom  
407 (Fig. 4c). This coincided with the hydrographic front between the PSW and the ambient  
408 water (Figs. 4a,b). *Våge et al.* [2013] proposed two possible mechanisms for the formation  
409 of the separated EGC. First, they demonstrated that the orography of Greenland, in  
410 combination with the predominantly northerly barrier winds [*Harden et al.*, 2011], results  
411 in negative wind stress curl across the Blosseville Basin. It was hypothesized that this,  
412 in combination with the closed isobaths of the basin, could spin up an anti-cyclonic gyre  
413 whose offshore branch is the separated EGC. The moored measurements of *Harden et al.*  
414 [2016] are consistent with this notion. The second hypothesis of *Våge et al.* [2013] for  
415 the formation of the separated EGC, based on idealized numerical simulations, is that  
416 baroclinic instability of the shelfbreak EGC at the northern end of the Blosseville Basin  
417 generates anti-cyclonic eddies that migrate offshore and coalesce as they encounter the  
418 base of the Iceland slope. In the model, this merging of eddies forms the offshore branch  
419 of the current.

420 In the southern part of our domain, in sections 2-5, both cyclonic and anti-cyclonic  
421 eddies were observed. The anti-cyclones typically had a core of Atlantic-origin Water,  
422 whereas the cyclones had a core of ambient water. The eddies were likely formed via

423 baroclinic instability of the shelfbreak EGC. This process should form dipole pairs: the  
424 anti-cyclone associated with the meandering of the current, and the weaker near-field  
425 cyclone adjacent to the meander. The latter features are displaced deeper in the water  
426 column and tend to wrap boundary current water around their edges (e.g. *Spall* [1995]).  
427 While eddies of both signs are formed initially (and are necessary for self advection off-  
428 shore), the cyclones tend to spin down more readily so that, in the far field, anti-cyclones  
429 typically dominate [*Lilly et al.*, 2003].

430 In section 3 we sampled a 30 km diameter cyclone close to the offshore edge of the  
431 shelfbreak EGC, centered near  $x = 100$  km where relatively cool and fresh ambient water  
432 interrupted the Atlantic-origin Water otherwise present in this part of the section (Fig.  
433 4a,b). Note the pinching of isopycnals near 100 m depth (e.g. the 27.8 and 27.95  $\text{kg/m}^3$   
434 density contours), consistent with the sub-surface maximum in velocity of this feature,  
435 versus the surface-intensified core of the shelfbreak EGC. The lateral boundary between  
436 the eddy and the boundary current was determined by balancing mass in the cyclone.  
437 *Våge et al.* [2013] identified a critical region north of Denmark Strait for the shedding  
438 of eddies from the shelfbreak EGC associated with the formation of the separated EGC.  
439 In their numerical simulations the eddies originated from the continental slope at the  
440 northern end of the Blosseville Basin near  $69^\circ\text{N}$  where there is a pronounced curvature  
441 in the bathymetry (Fig. 1). The eddies that were sampled on sections 2-5 are generally  
442 consistent with this idea that the separated EGC is formed by eddies coalescing along the  
443 base of the Iceland slope.

## 5. Transports

444 Our estimates of volume transport depend on the strength of the current as well as  
445 our semi-objective choice of the lateral bounds of the feature in question and how well  
446 it is sampled. Of the different components identified in the EGC system, the shelfbreak  
447 branch was the most important in terms of volume transport and also the best sampled.  
448 As such, we focus on the along-stream evolution of the volume transport of this part of  
449 the boundary current system.

### 5.1. Volume Transport of the Shelfbreak EGC

450 The large section-to-section variability in core speed and width of the shelfbreak EGC  
451 noted earlier (Fig. 6) indicates that the current is very dynamic. However, these two as-  
452 pects tend to offset each other to some degree, resulting in a more interpretable signal in  
453 volume transport. The current had a significant barotropic component and hence to esti-  
454 mate the total transport, measurements to the bottom would be required. Unfortunately  
455 this was not achieved in the two northernmost sections where the CTD casts extended  
456 only to 800 m depth (due to time constraints). In light of the fact that the bottom depth  
457 at some of the stations on these sections exceeded 3000 m, the total transports in sec-  
458 tions 9 and 10 are clearly underestimates. Even so, we include the partial estimates for  
459 completeness.

460 Taking into account the underestimated transports in the northern sections, it is evi-  
461 dent that the total transport of the shelfbreak EGC decreased from north to south, with  
462 variability about this trend (Fig. 6). Such a decrease is to be expected, since water is  
463 diverted from the boundary between Fram Strait and Denmark Strait (e.g. via the Jan  
464 Mayen Current [*Bourke et al.*, 1992], the East Icelandic Current [*Macranders et al.*, 2014],

465 and the bifurcation of the EGC in the Blosseville Basin). When calculating the mean vol-  
466 ume transport of the EGC using mooring data from the Greenland Sea, *Woodgate et al.*  
467 [1999] divided the transport estimates into a throughput and a recirculation according  
468 to whether the temperature was above or below 0 °C, respectively. The annual mean  
469 throughput estimated by *Woodgate et al.* [1999] was  $8 \pm 1$  Sv, which can be compared  
470 to our value of the transport above the lower 0 °C isotherm at sections 8 and 9 in the  
471 Greenland Sea of  $5.3 \pm 1.4$  Sv and  $5.7 \pm 0.95$  Sv, respectively. Our estimates are lower  
472 than theirs, but within the short-term variability exhibited in their time series. (The  
473 difference is not due to a sampling issue since the lower 0 °C isotherm was above 800 m  
474 in section 9.)

475 We apply the throughput definition of *Woodgate et al.* [1999] outside of the Greenland  
476 Sea as well as a means to isolate the part of the shelfbreak EGC that exits the Nordic  
477 Seas through Denmark Strait. Although the depth of the lower 0 °C isotherm is gener-  
478 ally deeper than the sill depth of Denmark Strait (650 m), *Harden et al.* [2016] recently  
479 demonstrated that a portion of the overflow water aspirates from depths greater than this.  
480 As shown below, the choice of the 0 °C isotherm appears to be realistic. We further par-  
481 tition the shelfbreak EGC transport into a surface layer contribution and an intermediate  
482 layer contribution, where the surface layer extends to the 27.7 kg/m<sup>3</sup> isopycnal and the  
483 intermediate layer extends from there to the deep 0 °C isotherm (as described in Section  
484 3). This reveals that there are different trends in the two different parts of the water  
485 column.

486 As seen in Fig. 6, the transport of surface water (which is completely captured in all  
487 of our sections) was more or less constant among the four northernmost sections at ap-



488 proximately  $1.2 \pm 0.1$  Sv, with a lower mean value around  $0.6 \pm 0.1$  Sv for the sections  
489 to the south. An offshore transport of surface waters in this area is supported both  
490 by observations, showing relatively fresh waters offshore of the shelfbreak in and north  
491 of the Blossville Basin, and by idealized numerical modeling showing eddies carrying  
492 near-surface EGC water offshore [Våge *et al.*, 2013]. By contrast, the transport of the  
493 intermediate water decreased steadily from north to south, with sections 4 and 2 having  
494 particularly low values (Fig. 6). This was a result of a very narrow current in section 4  
495 (not adequately compensated for by the strong velocity) and a region of northward veloc-  
496 ities within the shelfbreak part of the current in section 2. This highlights the inherent  
497 variability in a synoptic survey; indeed, mooring-based studies of the EGC (e.g. *Woodgate*  
498 *et al.* [1999]; *Harden et al.* [2016]) have indicated that individual realizations can differ  
499 significantly from long-term means.

500 The dense overflow water flowing through Denmark Strait is traditionally defined as  
501 having a density greater than  $27.8 \text{ kg/m}^3$  [Dickson and Brown, 1994], and previous trans-  
502 port estimates in the Iceland Sea (e.g. [Våge *et al.*, 2011, 2013]) have used the sill depth  
503 as the lower limit. Here we take the intermediate layer defined above as an approximate  
504 representation of the overflow water (noting that the difference in depth of the  $27.7$  and  
505  $27.8 \text{ kg/m}^3$  isopycnals in each of our sections is small). This results in a mean overflow  
506 water transport of  $2.8 \pm 0.7$  Sv, which is close to the annual mean value of  $2.54 \pm 0.16$  Sv  
507 obtained by *Harden et al.* [2016] at the location of section 2. This good agreement sup-  
508 ports our choice of the deep  $0 \text{ }^\circ\text{C}$  isotherm as the lower limit for the overflow water, and  
509 also suggests that any aspiration below this level is limited.

## 5.2. Freshwater Transport

510 Most of the freshwater sampled during the survey resided on the east Greenland shelf  
511 and in the shelfbreak EGC. Recall that only sections 2, 3, and 6 covered the entire  
512 shelf/EGC system (Fig. 1), so, for the other sections, the FWT was calculated only for  
513 the shelfbreak EGC. While the 34.8 isohaline shoaled to the east along each section, it only  
514 outcropped at the seaward end of section 9 (last station) and on section 10; hence some  
515 portion of the FWT relative to this isohaline occurred outside of most of the sections. The  
516 total calculated FWT ranged from a maximum of  $127 \pm 13$  mSv at section 6 to a minimum  
517 of  $81 \pm 8$  mSv at section 3 (Fig. 9). The FWT of the shelfbreak EGC, calculated for  
518 every section, revealed the same pattern as the volume transport of the surface layer with  
519 a clear decrease south of the Jan Mayen Fracture Zone. In the sections extending onto the  
520 shelf the FWT in the PSW Jet ranged between 29% of the total FWT (section 2) to 55%  
521 (section 3). Due to the very low presence of freshwater in the outer EGC the contribution  
522 from this branch was less than 5 mSv in sections 6 and 9, and close to 0 in section 10  
523 (not plotted in Fig. 9). In the two southern-most sections where the separated EGC was  
524 present, it contributed 25% and 37% to the total FWT, emphasizing the importance of  
525 the bifurcation in diverting freshwater into the interior. This partitioning of the FWT  
526 into the different branches of the EGC highlights the importance of sampling the entire  
527 width of the current system, in particular the full width of the shelf as the PSW Jet is  
528 responsible for a sizeable fraction of the FWT.

529 We compare our FWT estimates from section 2 and 3 to previous results based on ob-  
530 servations obtained along our section 2. All estimates are relative to a reference salinity  
531 of 34.8. *Våge et al.* [2013] calculated the FWT from 4 high-resolution transects obtained  
532 along this section. They divided the FWT between the shelfbreak branch and the sepa-

533 rated branch. The two branches contributed  $108 \pm 24$  mSv and  $29 \pm 7$  mSv, respectively.  
534 Their mean FWT in the shelfbreak branch was higher than ours, both as a result of syn-  
535 optic variability and due to the fact that they did not consider the PSW Jet a distinct  
536 branch. However, the relative contribution of the separated branch to the total FWT  
537 (25 %) was similar to our estimate (31 %).

538 The East Icelandic Current separates from the EGC between section 6 and the Blos-  
539 seville Basin. Recently *Macrander et al.* [2014] estimated the mean FWT in this cur-  
540 rent from a decade of observations at the Langanes section northeast of Iceland to be  
541  $3.4 \pm 0.3$  mSv (relative to a salinity of 34.93). This is an order of magnitude lower than  
542 the approximate 50 mSv reduction in FWT from section 6 to the Blosseville Basin cal-  
543 culated in our survey, suggesting that if the East Icelandic Current contributes to this  
544 reduction it would have to lose most of the FWT before reaching Langanes. (The dis-  
545 crepancy is not sensitive to the choice of reference salinity.) The mesoscale eddy activity  
546 south of the Jan Mayen Fracture Zone could transport freshwater off the boundary and  
547 contribute to a freshening of the western Iceland Sea, between the Kolbeinsey Ridge and  
548 the Greenland shelf. We assume that the observed eddies are symmetric and as long as  
549 we cover their entire width, our estimates of the total FWT is not susceptible to their  
550 presence. Also, we did not sample eddies on the offshore ends of the sections. We will  
551 return to the fate of the FWT diverted offshore in Section 7.

## 6. Along-stream Water Mass Modification

552 Thus far we have discussed water masses in terms of the three-layered structure in-  
553 troduced in Section 3: PSW, Atlantic-origin Water, and the lower-intermediate layer.  
554 Previous studies (e.g. *Rudels et al.* [2002, 2005]; *Jeansson et al.* [2008]) have presented

555 details of the water masses of the EGC system and how they are modified from Fram  
556 Strait to Denmark Strait. We do not attempt the same detailed analysis here, but rather  
557 focus on the along-stream modification of the Atlantic-origin Water, which has potential  
558 implications for the dense overflow water passing through Denmark Strait.

### 6.1. Modification of the Atlantic-origin Water

559 All of the CTD profiles in the survey with a temperature maximum above 0 °C below  
560 the 27.7 kg/m<sup>3</sup> isopycnal contained Atlantic-origin Water. These are shown in Fig. 10 in  
561 the  $\theta/S$  plane as a scatter plot, and are color-coded according to their section number.  
562 We also computed a single average profile for each section and these are included in Fig.  
563 10 as solid lines. Section 10 is unique in that there is a large amount of Atlantic-origin  
564 Water extending to the offshore end of the section, and, notably, this water mass was  
565 in direct contact with the atmosphere. By contrast, farther south a thin layer of PSW  
566 extended over most of each of the transects (compare Figs. 2 and 3). Combined with the  
567 fact that the Atlantic-origin Water generally becomes colder and less saline enroute from  
568 Fram Strait to Denmark Strait (Figs. 2, 3, and 4), this means that, in the northern part  
569 of the domain, the average  $\theta/S$  profiles are substantially warmer in the upper part of the  
570 water column (Fig. 10). This is most extreme at section 10 in Fram Strait.

571 We now focus on the along-stream change in hydrographic properties of the core of the  
572 Atlantic-origin Water, which allows us to assess the mixing that has taken place. For  
573 each CTD profile the core of the Atlantic-origin Water was identified by the intermediate  
574 temperature maximum. Fig. 11 shows the  $\theta/S$  properties of the core for the entire survey.  
575 In the quadrant marked “shelfbreak EGC”, the properties of the core were predominantly  
576 modified isopycnally (approximately along the 27.9 kg/m<sup>3</sup> isopycnal). The largest devi-

577 ation from this was found in some of the offshore profiles on section 10 where the core  
578 density was closer to  $27.8 \text{ kg/m}^3$ . Recall that the Atlantic-origin Water there was still in  
579 contact with the atmosphere; an additional cooling of  $0.5\text{-}1 \text{ }^\circ\text{C}$  would modify the water  
580 enough to reach the  $27.9 \text{ kg/m}^3$  density level. In the quadrant marked “offshore”, the  
581 Atlantic-origin Water seaward of the shelfbreak EGC was undergoing diapycnal mixing  
582 resulting in a change in temperature but only small changes in salinity. Finally, the “shelf”  
583 quadrant shows a tail towards low salinities corresponding to stations on the east Green-  
584 land shelf in sections 6, 3, and 2 that are strongly modified by the fresh PSW. We note that  
585 all the stations in the shelfbreak current are found in the quadrant marked “Shelfbreak  
586 EGC”, plus some offshore stations which contain relatively unmodified Atlantic-origin Wa-  
587 ter (see for example Fig. 2 where the warm Atlantic-origin Water had spread well east of  
588 the shelfbreak current.) In the other two quadrants the water is solely from the indicated  
589 region. We will consider in more detail the modification of the Atlantic-origin Water  
590 within and offshore of the shelfbreak EGC separately in Sections 6.1.1 and 6.1.2.

591 What water masses mixed with the Atlantic-origin Water in order to change its core  
592 properties as depicted in Fig. 11? The  $\theta/S$  diagram in Fig. 10 illustrates the end member  
593 water masses available for mixing. By drawing a mixing triangle it appears that nearly all  
594 of the hydrographic measurements can be represented by a combination of PSW, Atlantic  
595 Water, and a deep water mass. We note that this definition of the deep water mass is  
596 within historical definitions of intermediate waters such as the upper Polar Deep Water  
597 and Arctic Intermediate Water [*Rudels et al.*, 2005]; in the present context deep water  
598 refers to water denser than the Atlantic-origin Water. From these three end members  
599 we calculated their relative contributions to the Atlantic-origin core for each profile. The

600 resulting percentages of each end member showed large variability from station to station  
601 across the sections (Fig. 12), consistent with the variable core properties described above.  
602 PSW typically contributed around 10 %, with the exception of some locations on the  
603 shelf where it was more prominent (these also constitute the low salinity tail in Fig. 11).  
604 The deep water contribution became increasingly important toward the south, and the  
605 Atlantic Water fraction, which dominated in the north, was reduced to around 50 % in  
606 sections 2 and 3 (the PSW percentage was larger at the shoreward ends of these two  
607 sections). In sections 2-6 the region offshore of the shelfbreak EGC contained a larger  
608 fraction of deep water.

#### 609 **6.1.1. Atlantic-origin Water within the Shelfbreak EGC**

610 All of the Atlantic-origin core values within the shelfbreak EGC were characterized by  
611 a core temperature above 2 °C (all 8 sections were represented in this quadrant). In  
612 addition some of the profiles offshore of the shelfbreak current were characterized by the  
613 same relatively high temperature. Since the core properties of these profiles change in the  
614 same manner as those in the shelfbreak region, we focus the discussion on the stations  
615 within the shelfbreak current. In general this water cooled and freshened isopycnally  
616 as it progressed southward. However, core values as far south as section 4 had similar  
617 properties to the Atlantic Water sampled in Fram Strait (Fig. 11), demonstrating that  
618 some Atlantic Water can be advected with little modification from Fram Strait all the way  
619 to Blosseville Basin. This variability in the degree of along-stream isopycnal modification  
620 within the shelfbreak EGC could be due to sporadic mixing with the colder and fresher  
621 ambient waters stemming from the interior of the Greenland and Iceland Seas.

622 In order to explore this possibility, we constructed average profiles of temperature and  
623 salinity from each of the two seas using the historical database described in *Våge et al.*  
624 [2013] (not shown). By comparing the typical hydrographic properties at the  $27.9 \text{ kg/m}^3$   
625 isopycnal in the interior seas ( $\Theta = 0.7^\circ\text{C}$ ,  $S = 34.8$  in the Iceland Sea and  $\Theta = 1.2^\circ\text{C}$ ,  
626  $S = 34.8$  in the Greenland Sea) with the corresponding values in the shelfbreak EGC,  
627 the potential for isopycnal modification of the Atlantic-origin Water was evaluated. We  
628 found it unlikely that these interior waters influence the shelfbreak EGC (or even the  
629 offshore Atlantic-origin Water), for several reasons. This includes the fact that there is a  
630 significant mismatch in the hydrographic properties at the  $27.9 \text{ kg/m}^3$  isopycnal between  
631 the boundary current and the interior basins, and the fact that the  $27.9 \text{ kg/m}^3$  isopycnal  
632 outcrops quite far from the center of the basins over a large part of the year, hence  
633 preventing such an exchange. As an example, most of the Atlantic-origin Water within  
634 the shelfbreak current from section 5 and southward would need an addition of more  
635 than 50 % Iceland Sea water to obtain the observed core hydrographic properties. The  
636 Iceland Sea water mass is barely present in any of the casts on our sections, suggesting  
637 that it is not readily available for mixing with the Atlantic-origin Water in the core of  
638 the shelfbreak EGC. Similar mixing ratios are found in the Greenland Sea, though with  
639 larger variability from cast to cast.

640 In light of the end member calculation above, it seems more likely that the PSW and  
641 deep water mix with the Atlantic-origin Water in the shelfbreak EGC and modify it isopyc-  
642 nally as it progresses from Fram Strait to Denmark Strait. Notably, such modification  
643 along density surfaces supports the view, first proposed by *Mauritzen* [1996], that the

644 Atlantic-origin Water is mostly densified in the eastern part of the Nordic Seas via air-sea  
645 fluxes.

### 646 **6.1.2. Atlantic-origin Water offshore of the Shelfbreak EGC**

647 In the sections south of the Jan Mayen Fracture Zone (sections 2-6) the Atlantic-origin  
648 Water offshore of the shelfbreak EGC was modified diapycnally (lower right quadrant of  
649 Fig. 11). This was likely due to mixing with the deep water, considering the relatively  
650 high percentage of that water mass in these sections (Fig. 12). Interestingly, the off-  
651 shore Atlantic-origin Water salinity appeared to reach a threshold value, marked by the  
652 34.9 isohaline in Fig. 11. The depth of the temperature maximum in the Atlantic-origin  
653 Water was shallower offshore than within the shelfbreak EGC, even though the density  
654 was higher. This was due to the strong stratification in the top 50 m. Below that the  
655 intermediate salinity maximum, characteristic of the shelfbreak EGC, was largely eroded.

## 7. Discussion and Conclusions

656 A high-resolution hydrographic/velocity survey of the East Greenland Current (EGC),  
657 conducted in summer 2012, revealed that the current had three distinct branches: the  
658 shelfbreak EGC situated in the vicinity of the shelfbreak, the Polar Surface Water (PSW)  
659 Jet on the continental shelf, and the outer EGC over the mid to deep continental slope.  
660 In Fig. 13 we provide a schematic overview of the circulation in the Nordic Seas that  
661 includes these branches and their presumed upstream sources. Atlantic Water enters the  
662 Nordic Seas in the southeast both via the Iceland-Faroe and the Faroe-Shetland inflows  
663 [Hansen *et al.*, 2015]. Farther north this leads to two distinct branches that transport  
664 Atlantic Water poleward: the Norwegian Atlantic Slope Current (NwASC) following the  
665 continental shelfbreak offshore of Norway and the Norwegian Atlantic Frontal Current



666 (NwAFC) situated at the hydrographic front between the Atlantic Water in the Norwegian  
667 Sea and the colder and fresher water in the Greenland Sea [*Orvik and Niiler, 2002*].  
668 In Fram Strait the two branches appear to continue along different trajectories. The  
669 NwASC progresses northward toward the Arctic Ocean in the eastern branch of the WSC  
670 [*Beszczynska-Möller et al., 2012*], whereas the NwAFC constitutes the western branch of  
671 the WSC which recirculates in Fram Strait and forms the outer EGC. This recirculation  
672 provides a direct pathway for Atlantic Water across Fram Strait. Previous studies have  
673 shown that Atlantic Water is also fluxed westwards in the northern part of Fram Strait  
674 by extensive eddy activity, subsequently merging with the shelfbreak EGC [*von Appen*  
675 *et al., 2016; Hattermann et al., 2016*].

676 The outer EGC and the shelfbreak EGC flow equatorward side-by-side at least as far  
677 south as the Jan Mayen Fracture Zone. Along this pathway the volume transport of  
678 the outer EGC decreases. This gradual disintegration might be a result of baroclinic  
679 instability, similar to what is believed to take place in the western Arctic boundary current  
680 [*von Appen and Pickart, 2012*]. On the other hand, our sampling could be biased due  
681 to temporal variability. In the Blosseville Basin the separated EGC is associated with  
682 a similar baroclinic front as the outer EGC, and they could potentially be connected.  
683 However, this is not evident from our survey. Also, the separated EGC carries an order  
684 of magnitude more freshwater than the outer EGC. At sections 9 and 10 the outer EGC  
685 was directed along the shelf break, whereas a more southeastward direction was observed  
686 at section 6 (Fig. 5). This could indicate an offshore veering of the current towards the  
687 Iceland Sea south of section 6. In summary, the fate of the outer EGC south of the  
688 Jan Mayen Fracture Zone is not clear and it remains an open question as to whether

689 it disintegrates, continues equatorward towards Denmark Strait, or is diverted into the  
690 Iceland Sea.

691 A portion of the surface water in the shelfbreak EGC is fluxed offshore in the Jan Mayen  
692 and East Icelandic Currents (Fig. 13). In the northern end of the Blosseville Basin the  
693 above-mentioned bifurcation diverts both surface water and denser intermediate water  
694 offshore into the separated EGC. Upstream of Denmark Strait the separated EGC partly  
695 merges with the North Icelandic Jet which transports water originating from intermediate  
696 depths in the Iceland Sea [Våge *et al.*, 2011; Harden *et al.*, 2016]. To complete the overview  
697 of the circulation in the Nordic Seas, we have also included the inflowing North Icelandic  
698 Irminger Current (NIIC) which transports Atlantic Water northward through Denmark  
699 Strait and into the Iceland Sea.

700 The PSW Jet, indicated as a separate current branch on the Greenland continental shelf  
701 in Fig. 13, is responsible for a substantial fraction of the FWT (more than 50 % in one of  
702 the three sections). Unfortunately we have no means of evaluating whether this branch is  
703 present throughout the year. Köhl *et al.* [2007] presented a 3-year mean meridional section  
704 across the EGC close to 68°N from a numerical model where a substantial southward  
705 transport takes place on the shelf. However, they did not elaborate upon the temporal  
706 variation of this feature. Due to its origin on the Greenland shelf and its relationship to  
707 the density gradients of PSW, the PSW Jet may be most important in summer when the  
708 pool of freshwater on the shelf increases due to runoff from Greenland and ice melt. This  
709 could increase the cross-shelf density gradient and strengthen the PSW Jet.

710 Between section 6 and the Blosseville Basin the total FWT of the EGC system decreased  
711 significantly, but it is not clear what caused this decrease. At least two scenarios are

712 possible. Either the FWT could be diverted into the western Iceland Sea west of the  
713 Kolbeinsey Ridge, or it could be advected into the central Iceland Sea by the East Icelandic  
714 Current. In the second scenario the mismatch between the estimates of FWT in the EIC  
715 at the Langanes section northeast of Iceland [*Macrander et al.*, 2014] and the decrease  
716 in FWT measured here suggests that, if the freshwater is transported into the Iceland  
717 Sea, it does not reach as far east as Langanes and instead penetrates into the Iceland  
718 Sea. The northwestern corner of the Iceland Sea has been identified as a possible source  
719 region for the densest waters formed by wintertime convection that supply the NIJ [*Våge*  
720 *et al.*, 2015]. The preconditioning for convection in this area is likely influenced by the  
721 offshore diversion of both fresh surface waters and Atlantic-origin Water from the EGC.  
722 The freshwater could inhibit convection due to the increased surface stratification, or,  
723 if it takes part in convection, could be sequestered at depth. Either way the fate of the  
724 freshwater can potentially have important implications for the formation and hydrographic  
725 properties of the dense water supplying the Denmark Strait Overflow.

726 The shelfbreak EGC carries both light surface water from the Arctic Ocean and denser  
727 intermediate water masses. This current branch was the major source of dense water  
728 from the EGC to the Denmark Strait Overflow, with an average transport of  $2.8 \pm 0.7$  Sv.  
729 With a nearly isopycnal along-stream modification of the Atlantic-origin Water from Fram  
730 Strait to Denmark Strait, the density of the overflow water was not very sensitive to these  
731 hydrographic changes. As a result, the presence of relatively unmodified water from Fram  
732 Strait in the northern Blosseville Basin did not affect the local density of the overflow  
733 directly. However, due to the differing effect of pressure on warm and cold water, the  
734 density at depth in the North Atlantic would be greatest for the overflow water that was

735 most strongly modified, i.e. the coldest variant. Hence, even though a warmer and more  
736 saline overflow layer has a similar density locally, it may not reach the same equilibrium  
737 depth after crossing the sill and sinking.

738 With the large section-to-section variability measured in our EGC survey, it is evident  
739 that the transport estimates presented here must be treated with some caution. Nev-  
740 ertheless, the high-resolution hydrography and velocity observations have allowed us to  
741 present synoptic flux estimates associated with all three branches of the EGC system,  
742 as they progress from Fram Strait to Denmark Strait. These are the first summertime  
743 estimates since the RV Oden expedition in 2002 [*Rudels et al.*, 2005; *Nilsson et al.*, 2008],  
744 and the first based on absolute geostrophic velocities. Our results have shed light on  
745 the circulation of Atlantic-origin Water in the Nordic Seas from south of Fram Strait to  
746 Denmark Strait, and, at the same time, have identified several open questions for further  
747 study.

748 **Acknowledgments.** Support for this work was provided by the Norwegian Research  
749 Council under Grant agreement no. 231647 (LH and KV), and the European Union 7th  
750 framework Programme (FP7 2007-2013) under Grant agreement no. 308299 NACLIM  
751 Project (KV). Funding was also provided by the US National Science Foundation un-  
752 der grant OCE-0959381 (RP). The data from the RRS James Clark Ross survey can be  
753 obtained from <http://kogur.whoi.edu>. CTD data from RV Oceania cruises can be re-  
754 trieved from the IOPAN data base or requested directly from [abesz@iopan.gda.pl](mailto:abesz@iopan.gda.pl). The  
755 data obtained from Pangaea.de were collected by the Alfred Wegner Institute and the  
756 Norwegian Polar Institute (cruises ARK XIV/2, ARK XV/3, LA97/2, LA02, LA03/12,  
757 and LA04/15).

## References

- 758 Aksenov, Y., S. Bacon, A. C. Coward, and A. G. Nurser (2010), The North Atlantic  
759 inflow to the Arctic Ocean: High-resolution model study, *Journal of Marine Systems*,  
760 79(1–2), 1–22, doi:10.1016/j.jmarsys.2009.05.003.
- 761 Bacon, S., G. Reverdin, I. G. Rigor, and H. M. Snaith (2002), A freshwater jet on the  
762 east Greenland shelf, *J. Geophys. Res.*, 107(C7), doi:10.1029/2001JC000935.
- 763 Bacon, S., P. G. Myers, B. Rudels, and D. A. Sutherland (2008), *Accessing the Inaccessible:*  
764 *Buoyancy-Driven Coastal Currents on the Shelves of Greenland and Eastern Canada*,  
765 pp. 703–722, Springer Netherlands, Dordrecht, doi:10.1007/978-1-4020-6774-7\_29.
- 766 Bacon, S., A. Marshall, N. P. Holliday, Y. Aksenov, and S. R. Dye (2014), Seasonal  
767 variability of the East Greenland Coastal Current, *Journal of Geophysical Research:*  
768 *Oceans*, 119(6), 3967–3987, doi:10.1002/2013JC009279.
- 769 Beszczynska-Möller, A., E. Fahrbach, U. Schauer, and E. Hansen (2012), Variability in  
770 Atlantic water temperature and transport at the entrance to the Arctic Ocean, 1997-  
771 2010, *ICES Journal of Marine Science: Journal du Conseil*, doi:10.1093/icesjms/fss056.
- 772 Bourke, R. H., A. M. Weigel, and R. G. Paquette (1988), The westward turning branch  
773 of the West Spitsbergen Current, *Journal of Geophysical Research: Oceans*, 93(C11),  
774 14,065–14,077, doi:10.1029/JC093iC11p14065.
- 775 Bourke, R. H., R. G. Paquette, and R. F. Blythe (1992), The Jan Mayen Current of  
776 the Greenland Sea, *Journal of Geophysical Research: Oceans*, 97(C5), 7241–7250, doi:  
777 10.1029/92JC00150.
- 778 de Steur, L., E. Hansen, R. Gerdes, M. Karcher, E. Fahrbach, and J. Holfort (2009),  
779 Freshwater fluxes in the East Greenland Current: A decade of observations, *Geophysical*

- 780 *Research Letters*, 36(23), doi:10.1029/2009GL041278.
- 781 de Steur, L., E. Hansen, C. Mauritzen, A. Beszczynska-Möller, and E. Fahrbach (2014),  
782 Impact of recirculation on the East Greenland Current in Fram Strait: Results from  
783 moored current meter measurements between 1997 and 2009, *Deep Sea Research Part*  
784 *I: Oceanographic Research Papers*, 92, 26 – 40, doi:10.1016/j.dsr.2014.05.018.
- 785 de Steur, L., R. S. Pickart, D. J. Torres, and H. Valdimarsson (2015), Recent changes  
786 in the freshwater composition east of Greenland, *Geophysical Research Letters*, 42(7),  
787 2326–2332, doi:10.1002/2014GL062759.
- 788 Dickson, R. R., and J. Brown (1994), The production of North Atlantic Deep Wa-  
789 ter: Sources, rates, and pathways, *Journal of Geophysical Research: Oceans*, 99(C6),  
790 12,319–12,341, doi:10.1029/94JC00530.
- 791 Egbert, G. D., and S. Y. Erofeeva (2002), Efficient Inverse Modeling of Barotropic  
792 Ocean Tides, *Journal of Atmospheric and Oceanic Technology*, 19(2), 183–204, doi:  
793 10.1175/1520-0426(2002)019<0183:EIMOBO>2.0.CO;2.
- 794 Fahrbach, E., J. Meincke, S. Østerhus, G. Rohardt, U. Schauer, V. Tverberg, and J. Ver-  
795 duin (2001), Direct measurements of volume transports through Fram Strait, *Polar*  
796 *Research*, 20(2), 217–224, doi:10.1111/j.1751-8369.2001.tb00059.x.
- 797 Haine, T. W., et al. (2015), Arctic freshwater export: Status, mechanisms, and prospects,  
798 *Global and Planetary Change*, 125, 13 – 35, doi:10.1016/j.gloplacha.2014.11.013.
- 799 Hansen, B., and S. Østerhus (2000), North Atlantic-Nordic Seas exchanges, *Progress in*  
800 *Oceanography*, 45(2), 109 – 208, doi:10.1016/S0079-6611(99)00052-X.
- 801 Hansen, B., K. M. H. Larsen, H. Hátún, R. Kristiansen, E. Mortensen, and S. Østerhus  
802 (2015), Transport of volume, heat, and salt towards the Arctic in the Faroe Current

- 803 1993-2013, *Ocean Science*, 11(5), 743–757, doi:10.5194/os-11-743-2015.
- 804 Hansen, E. (2006a), Physical oceanography during LANCE cruise LA02. Norwegian Polar  
805 Institute, Tromsø, doi:10.1594/PANGAEA.512016.
- 806 Hansen, E. (2006b), Physical oceanography during LANCE cruise LA03/12. Norwegian  
807 Polar Institute, Tromsø, doi:10.1594/PANGAEA.524746.
- 808 Hansen, E. (2006c), Physical oceanography during LANCE cruise LA04/15. Norwegian  
809 Polar Institute, Tromsø, doi:10.1594/PANGAEA.525956.
- 810 Harden, B. E., I. A. Renfrew, and G. N. Petersen (2011), A climatology of wintertime  
811 barrier winds off southeast Greenland, *Journal of Climate*, 24(17), 4701–4717, doi:  
812 10.1175/2011JCLI4113.1.
- 813 Harden, B. E., et al. (2016), Upstream Sources of the Denmark Strait Overflow: Observa-  
814 tions from a High-Resolution Mooring Array, *Deep Sea Research Part I: Oceanographic  
815 Research Papers*, 112, 94–112, doi:10.1016/j.dsr.2016.02.007.
- 816 Hattermann, T., P. E. Isachsen, W.-J. von Appen, J. Albrechtsen, and A. Sundfjord (2016),  
817 Eddy-driven recirculation of Atlantic Water in Fram Strait, *Geophysical Research Let-  
818 ters*, 43(7), 3406–3414, doi:10.1002/2016GL068323.
- 819 Holfort, J., and J. Meincke (2005), Time series of freshwater-transport on the East  
820 Greenland Shelf at 74°N, *Meteorologische Zeitschrift*, 14(6), 703–710, doi:10.1127/0941-  
821 2948/2005/0079.
- 822 Holfort, J., E. Hansen, S. Østerhus, S. Dye, S. Jónsson, J. Meincke, J. Mortensen,  
823 and M. Meredith (2008), *Freshwater Fluxes East of Greenland*, pp. 263–287, Springer  
824 Netherlands, Dordrecht, doi:10.1007/978-1-4020-6774-7\_12.

- 825 Isachsen, P. E., C. Mauritzen, and H. Svendsen (2007), Dense water formation in the  
826 Nordic Seas diagnosed from sea surface buoyancy fluxes , *Deep Sea Research Part I:  
827 Oceanographic Research Papers*, 54(1), 22 – 41, doi:10.1016/j.dsr.2006.09.008.
- 828 Jeansson, E., S. Jutterström, B. Rudels, L. G. Anderson, K. A. Olsson, E. P. Jones,  
829 W. M. Smethie, and J. H. Swift (2008), Sources to the East Greenland Current and its  
830 contribution to the Denmark Strait Overflow, *Progress in Oceanography*, 78(1), 12–28,  
831 doi:10.1016/j.pocean.2007.08.031.
- 832 Jochumsen, K., D. Quadfasel, H. Valdimarsson, and S. Jónsson (2012), Variability of the  
833 Denmark Strait overflow: Moored time series from 1996-2011, *Journal of Geophysical  
834 Research: Oceans*, 117(C12), doi:10.1029/2012JC008244.
- 835 Köhl, A., R. H. Käse, D. Stammer, and N. Serra (2007), Causes of Changes in the  
836 Denmark Strait Overflow, *Journal of Physical Oceanography*, 37(6), 1678–1696, doi:  
837 10.1175/JPO3080.1.
- 838 Lilly, J. M., P. B. Rhines, F. Schott, K. Lavender, J. Lazier, U. Send, and E. DAsaro  
839 (2003), Observations of the Labrador Sea eddy field , *Progress in Oceanography*, 59(1),  
840 75 – 176, doi:10.1016/j.pocean.2003.08.013.
- 841 Macrander, A., H. Valdimarsson, and S. Jónsson (2014), Improved transport estimate of  
842 the East Icelandic Current 2002-2012, *Journal of Geophysical Research: Oceans*, 119(6),  
843 3407–3424, doi:10.1002/2013JC009517.
- 844 Manley, T. O. (1995), Branching of Atlantic Water within the Greenland-Spitsbergen Pas-  
845 sage: An estimate of recirculation, *Journal of Geophysical Research: Oceans*, 100(C10),  
846 20,627–20,634, doi:10.1029/95JC01251.



- 847 Marnela, M., B. Rudels, M.-N. Houssais, A. Beszczynska-Möller, and P. B. Eriksson  
848 (2013), Recirculation in the Fram Strait and transports of water in and north of the  
849 Fram Strait derived from CTD data, *Ocean Science*, *9*(3), 499–519, doi:10.5194/os-9-  
850 499-2013.
- 851 Mauritzen, C. (1996), Production of dense overflow waters feeding the North Atlantic  
852 across the Greenland-Scotland Ridge. Part 1: Evidence for a revised circulation  
853 scheme, *Deep Sea Research Part I: Oceanographic Research Papers*, *43*(6), 769–806,  
854 doi:10.1016/0967-0637(96)00037-4.
- 855 Nilsson, J., G. Björk, B. Rudels, P. Winsor, and D. Torres (2008), Liquid freshwa-  
856 ter transport and Polar Surface Water characteristics in the East Greenland Current  
857 during the AO-02 Oden expedition, *Progress in Oceanography*, *78*(1), 45 – 57, doi:  
858 10.1016/j.pocean.2007.06.002.
- 859 Nurser, A. J. G., and S. Bacon (2014), The Rossby radius in the Arctic Ocean, *Ocean*  
860 *Science*, *10*(6), 967–975, doi:10.5194/os-10-967-2014.
- 861 Orvik, K. A., and P. Niiler (2002), Major pathways of Atlantic water in the northern  
862 North Atlantic and Nordic Seas toward Arctic, *Geophysical Research Letters*, *29*(19),  
863 doi:10.1029/2002GL015002.
- 864 Paquette, R. G., R. H. Bourke, J. F. Newton, and W. F. Perdue (1985), The East Green-  
865 land Polar Front in autumn, *Journal of Geophysical Research: Oceans*, *90*(C3), 4866–  
866 4882, doi:10.1029/JC090iC03p04866.
- 867 Pickart, R. S., and W. M. Smethie (1998), Temporal evolution of the deep western bound-  
868 ary current where it enters the sub-tropical domain , *Deep Sea Research Part I: Oceanographic*  
869 *Research Papers*, *45*(7), 1053 – 1083, doi:10.1016/S0967-0637(97)00084-8.

- 870 Quadfasel, D., J.-C. Gascard, and K.-P. Koltermann (1987), Large-scale oceanography  
871 in Fram Strait during the 1984 Marginal Ice Zone Experiment, *Journal of Geophysical*  
872 *Research: Oceans*, 92(C7), 6719–6728, doi:10.1029/JC092iC07p06719.
- 873 Rabe, B., U. Schauer, A. Mackensen, M. Karcher, E. Hansen, and A. Beszczynska-Möller  
874 (2009), Freshwater components and transports in the Fram Strait – recent observations  
875 and changes since the late 1990s, *Ocean Science*, 5(3), 219–233, doi:10.5194/os-5-219-  
876 2009.
- 877 Rabe, B., et al. (2013), Liquid export of Arctic freshwater components through the Fram  
878 Strait 1998-2011, *Ocean Science*, 9(1), 91–109, doi:10.5194/os-9-91-2013.
- 879 Rudels, B., E. Fahrbach, J. Meincke, G. Budéus, and P. Eriksson (2002), The East Green-  
880 land Current and its contribution to the Denmark Strait overflow, *ICES Journal of*  
881 *Marine Science: Journal du Conseil*, 59(6), 1133–1154, doi:10.1006/jmsc.2002.1284.
- 882 Rudels, B., G. Björk, J. Nilsson, P. Winsor, I. Lake, and C. Nohr (2005), The interaction  
883 between waters from the Arctic Ocean and the Nordic Seas north of Fram Strait and  
884 along the East Greenland Current: results from the Arctic Ocean-02 Oden expedition,  
885 *Journal of Marine Systems*, 55(1), 1–30, doi:10.1016/j.jmarsys.2004.06.008.
- 886 Schauer, U. (2010), Physical oceanography during POLARSTERN cruise ARK-XV/3. Al-  
887 fredo Wegener Institute, Helmholtz Center for Polar and Marine Research, Bremerhaven,  
888 doi:10.1594/PANGAEA.742657.
- 889 Schauer, U., and G. Budéus (2010), Physical oceanography during POLARSTERN cruise  
890 ARK-XIV/2. Alfred Wegener Institute, Helmholtz Center for Polar and Marine Re-  
891 search, Bremerhaven, doi:10.1594/PANGAEA.742655.

- 892 Schauer, U., and G. Rohardt (2010), Physical oceanography during LANCE cruise  
893 LA97/2. Alfred Wegener Institute, Helmholtz Center for Polar and Marine Research,  
894 Bremerhaven, doi:10.1594/PANGAEA.742622.
- 895 Seidov, D., et al. (2015), Oceanography north of 60°N from World Ocean Database,  
896 *Progress in Oceanography*, 132, 153 – 173, doi:10.1016/j.pocean.2014.02.003.
- 897 Spall, M. A. (1995), Frontogenesis, subduction, and cross-front exchange at upper  
898 ocean fronts, *Journal of Geophysical Research: Oceans*, 100(C2), 2543–2557, doi:  
899 10.1029/94JC02860.
- 900 Strass, V. H., E. Fahrbach, U. Schauer, and L. Sellmann (1993), Formation of Denmark  
901 Strait overflow water by mixing in the East Greenland Current, *Journal of Geophysical*  
902 *Research: Oceans (1978–2012)*, 98(C4), 6907–6919.
- 903 Sutherland, D. A. (2008), The East Greenland Coastal Current: its structure variability,  
904 and large-scale impact, Ph.D. thesis, Massachusetts Institute of Technology and Woods  
905 Hole Oceanographic Institution.
- 906 Sutherland, D. A., and R. S. Pickart (2008), The East Greenland Coastal Current:  
907 Structure, variability, and forcing, *Progress in Oceanography*, 78(1), 58 – 77, doi:  
908 10.1016/j.pocean.2007.09.006.
- 909 Våge, K., R. S. Pickart, M. A. Spall, H. Valdimarsson, S. Jónsson, D. J. Torres, S. Øster-  
910 hus, and T. Eldevik (2011), Significant role of the North Icelandic Jet in the for-  
911 mation of Denmark Strait overflow water, *Nature Geoscience*, 4(10), 723–727, doi:  
912 10.1038/NGEO1234.
- 913 Våge, K., R. S. Pickart, M. A. Spall, G. Moore, H. Valdimarsson, D. J. Torres, S. Y.  
914 Erofeeva, and J. E. Ø. Nilsen (2013), Revised circulation scheme north of the Denmark

- 915 Strait, *Deep Sea Research Part I: Oceanographic Research Papers*, 79, 20 – 39, doi:  
916 10.1016/j.dsr.2013.05.007.
- 917 Våge, K., G. Moore, S. Jónsson, and H. Valdimarsson (2015), Water mass transformation  
918 in the Iceland Sea, *Deep Sea Research Part I: Oceanographic Research Papers*, 101, 98  
919 – 109, doi:10.1016/j.dsr.2015.04.001.
- 920 von Appen, W.-J., and R. S. Pickart (2012), Two Configurations of the Western Arctic  
921 Shelfbreak Current in Summer, *Journal of Physical Oceanography*, 42(3), 329–351, doi:  
922 10.1175/JPO-D-11-026.1.
- 923 von Appen, W.-J., U. Schauer, T. Hattermann, and A. Beszczynska-Möller (2016), Sea-  
924 sonal Cycle of Mesoscale Instability of the West Spitsbergen Current, *Journal of Physical*  
925 *Oceanography*, 46(4), 1231–1254, doi:10.1175/JPO-D-15-0184.1.
- 926 Walczowski, W. (2013), Frontal structures in the West Spitsbergen Current margins,  
927 *Ocean Science*, 9(6), 957–975, doi:10.5194/os-9-957-2013.
- 928 Walczowski, W., and J. Piechura (2007), Pathways of the Greenland Sea warming, *Geo-*  
929 *physical Research Letters*, 34(10), doi:10.1029/2007GL029974.
- 930 Woodgate, R. A., E. Fahrbach, and G. Rohardt (1999), Structure and transports of the  
931 East Greenland Current at 75°N from moored current meters, *Journal of Geophysical*  
932 *Research: Oceans*, 104(C8), 18,059–18,072, doi:10.1029/1999JC900146.

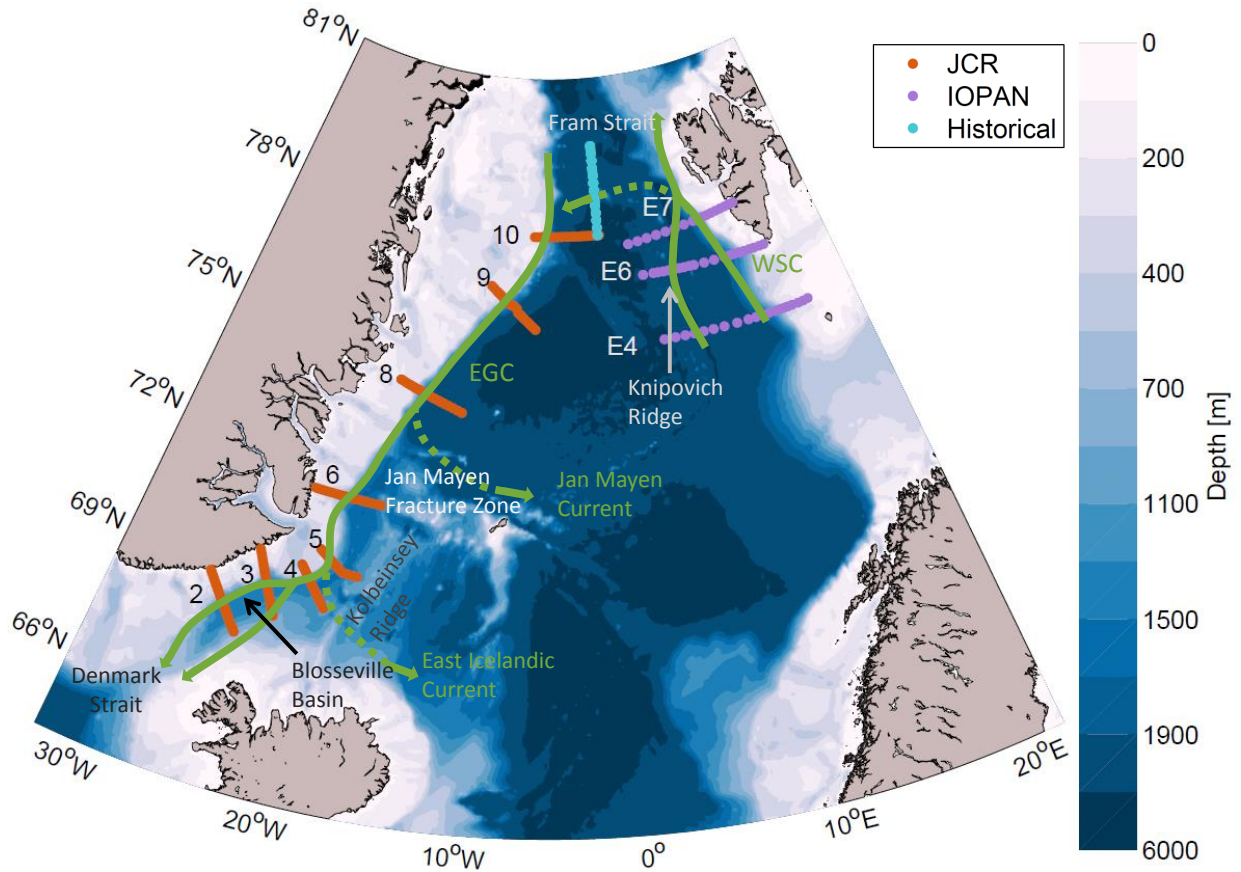


**Figure 1.** Location of the sections occupied during the two shipboard surveys in summer 2012 and the composite meridional section obtained from historical data in Fram Strait. The main currents discussed in the Introduction are sketched in green. In the Blosseville Basin the EGC bifurcates into the shelfbreak branch and the separated branch. Bathymetric features and geographical locations discussed in the text are indicated on the map. The bathymetry was obtained from the 2-minute resolution Etopo2 product.

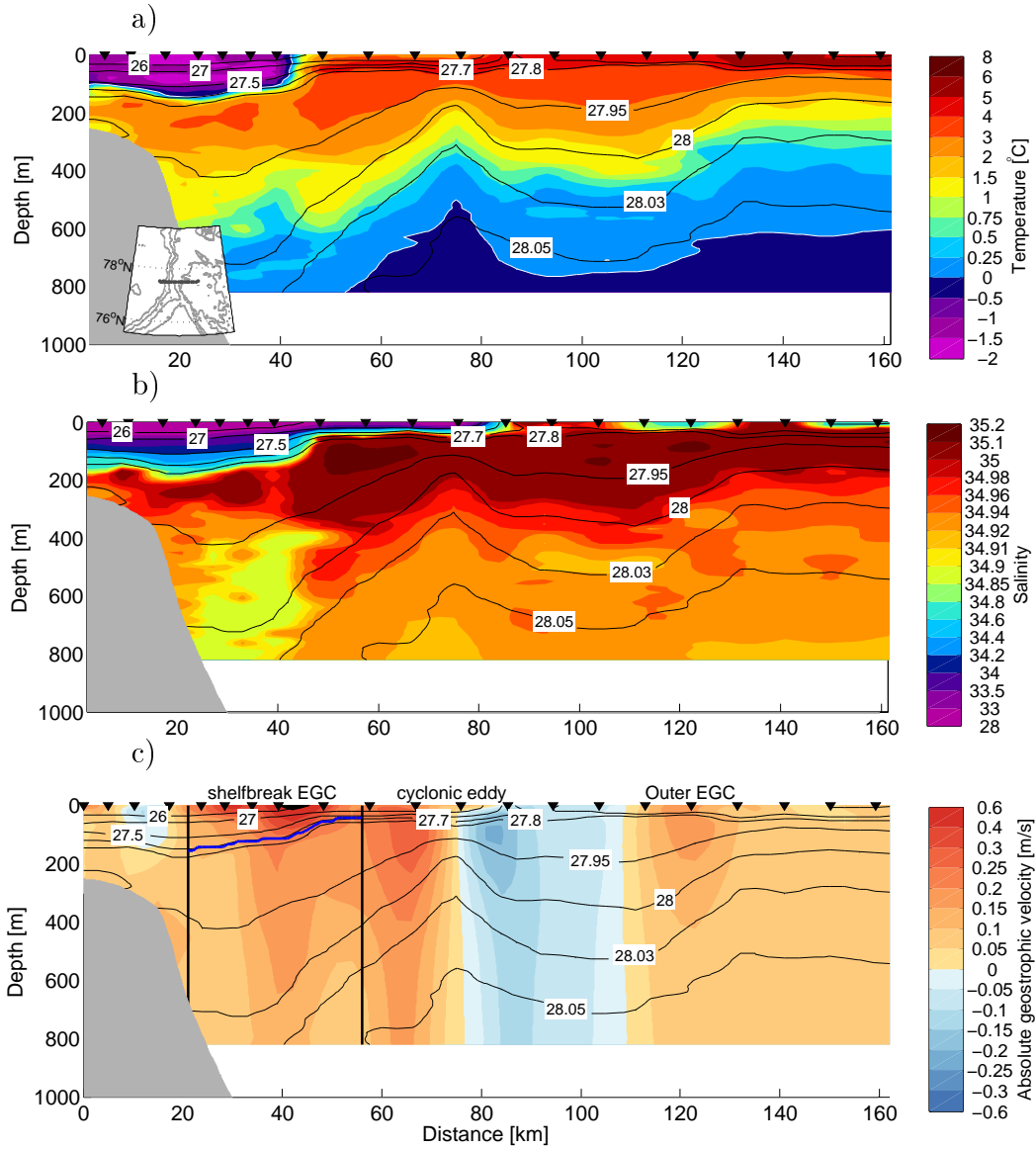


**Figure 2.** Vertical sections of (a) potential temperature, (b) salinity, and (c) absolute geostrophic velocity with contours of potential density ( $\text{kg}/\text{m}^3$ ), for section 10 in Fram Strait. The location of the section is shown in the inset in (a). Positive velocities are towards the south. The black inverted triangles along the top of each panel indicate the station locations. The white contours in (a) represent the  $0^\circ\text{C}$  isotherm. The black vertical lines in (c) enclose the shelfbreak branch of the EGC (see the text for details on how this branch was defined). The blue contour in (c) is the  $27.7 \text{ kg}/\text{m}^3$  isopycnal which separates the surface layer from the intermediate layer.

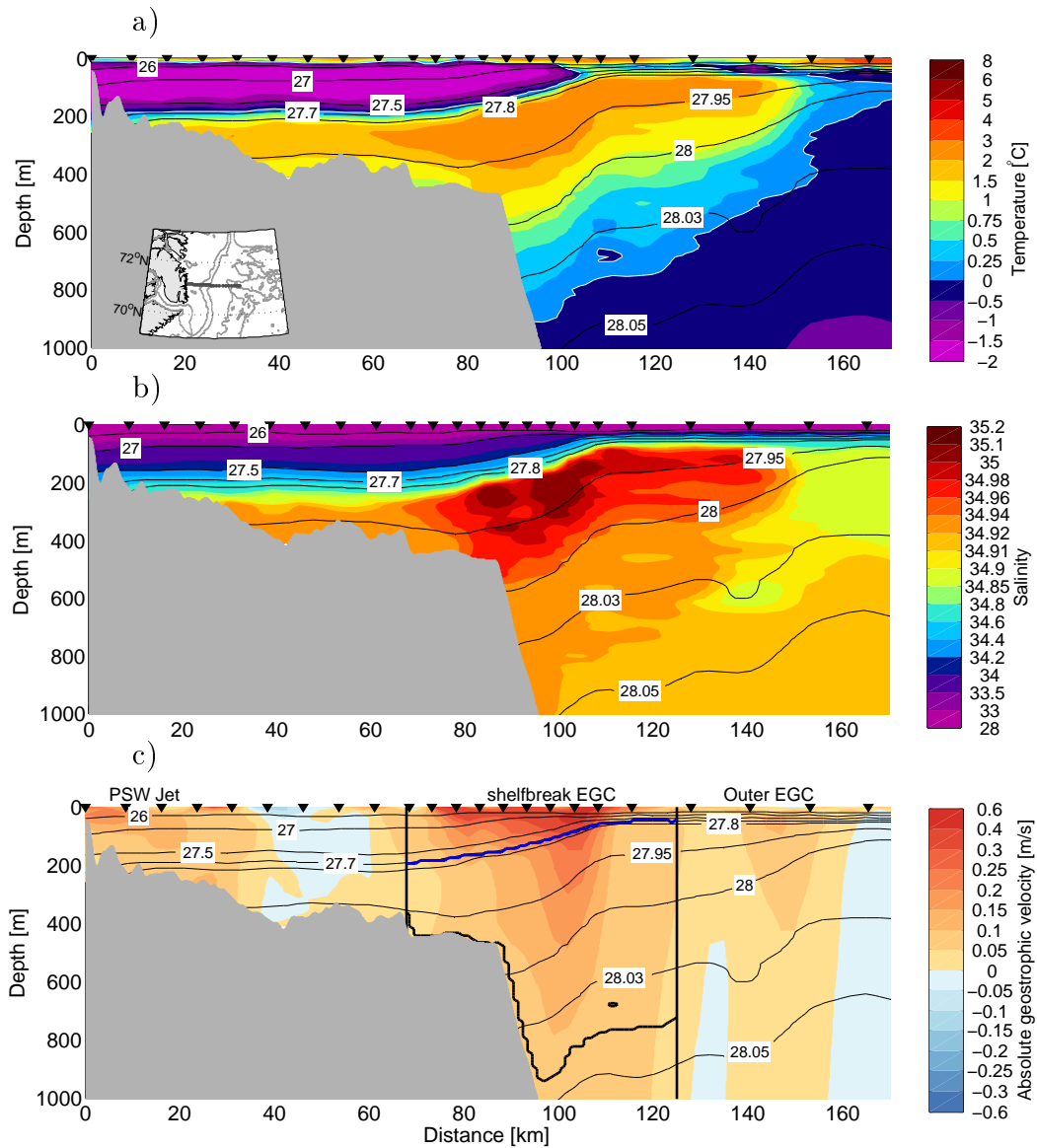


**Figure 3.** Vertical sections of hydrography and velocity for section 6 near the Jan Mayen Fracture Zone, otherwise as Fig. 2. The lower limit for the Atlantic-origin Water in the shelfbreak EGC is marked by the thick black contour (section 10 did not extend deep enough to capture this).

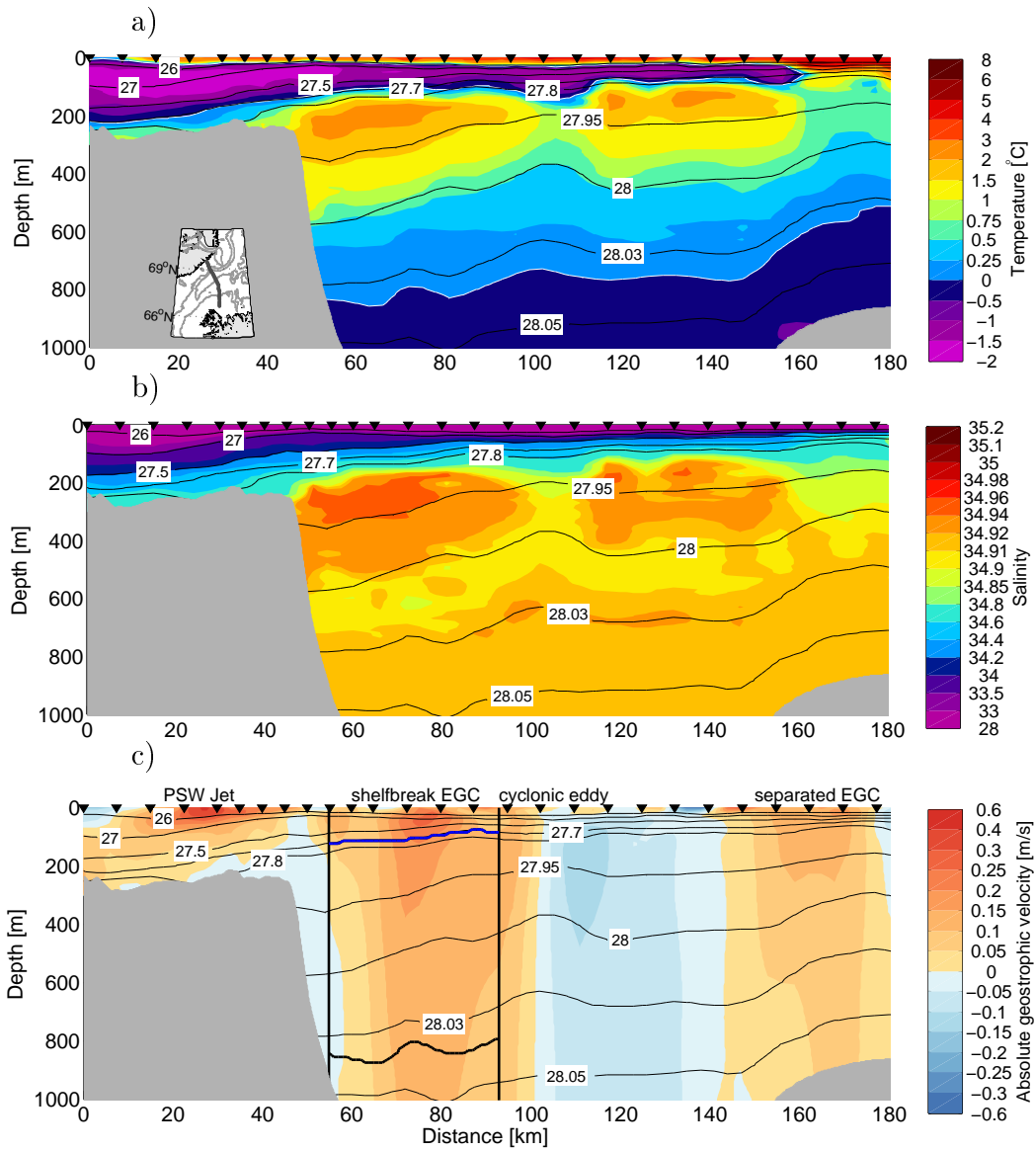


**Figure 4.** Vertical sections of hydrography and velocity for section 3 in the Blosseville Basin, otherwise as Fig. 3.



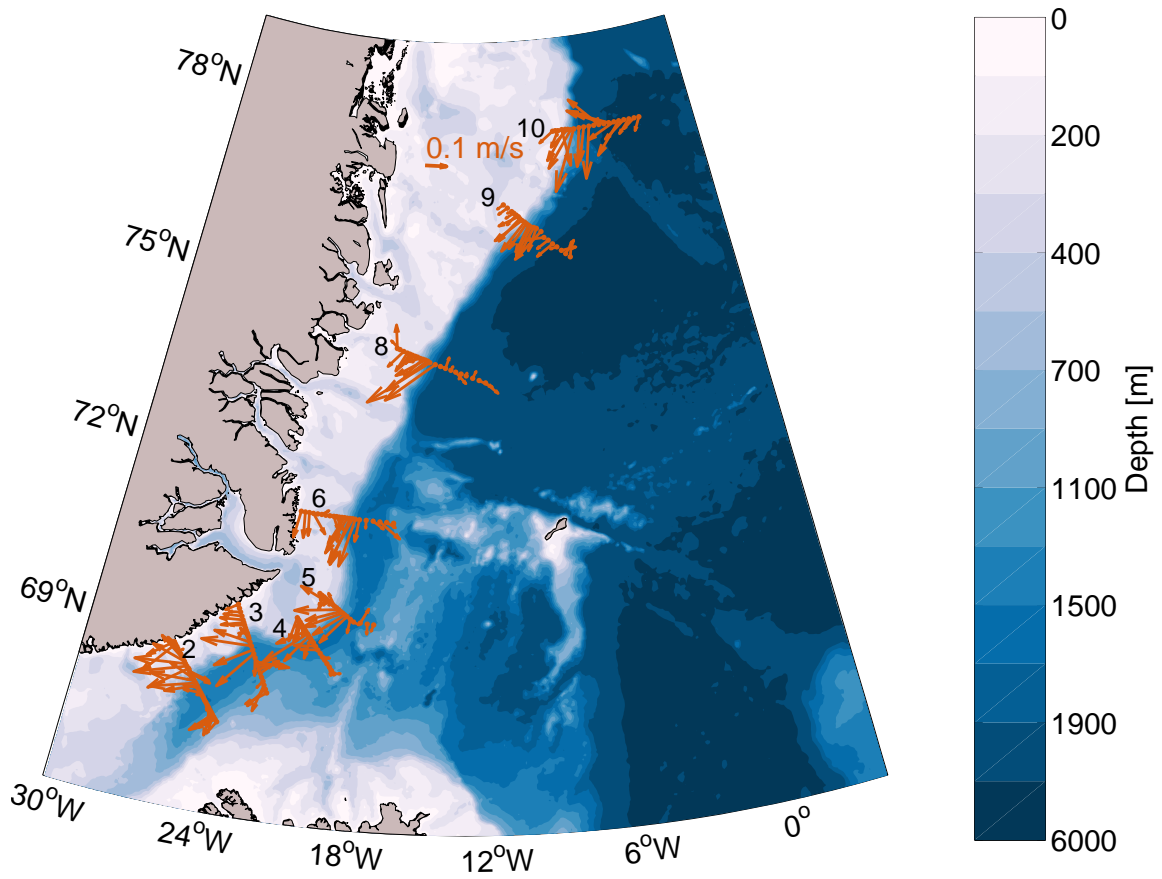


**Figure 5.** Depth-integrated velocity vectors for the upper 500 m at each station. For stations at shallower depths the integration was made to the bottom.

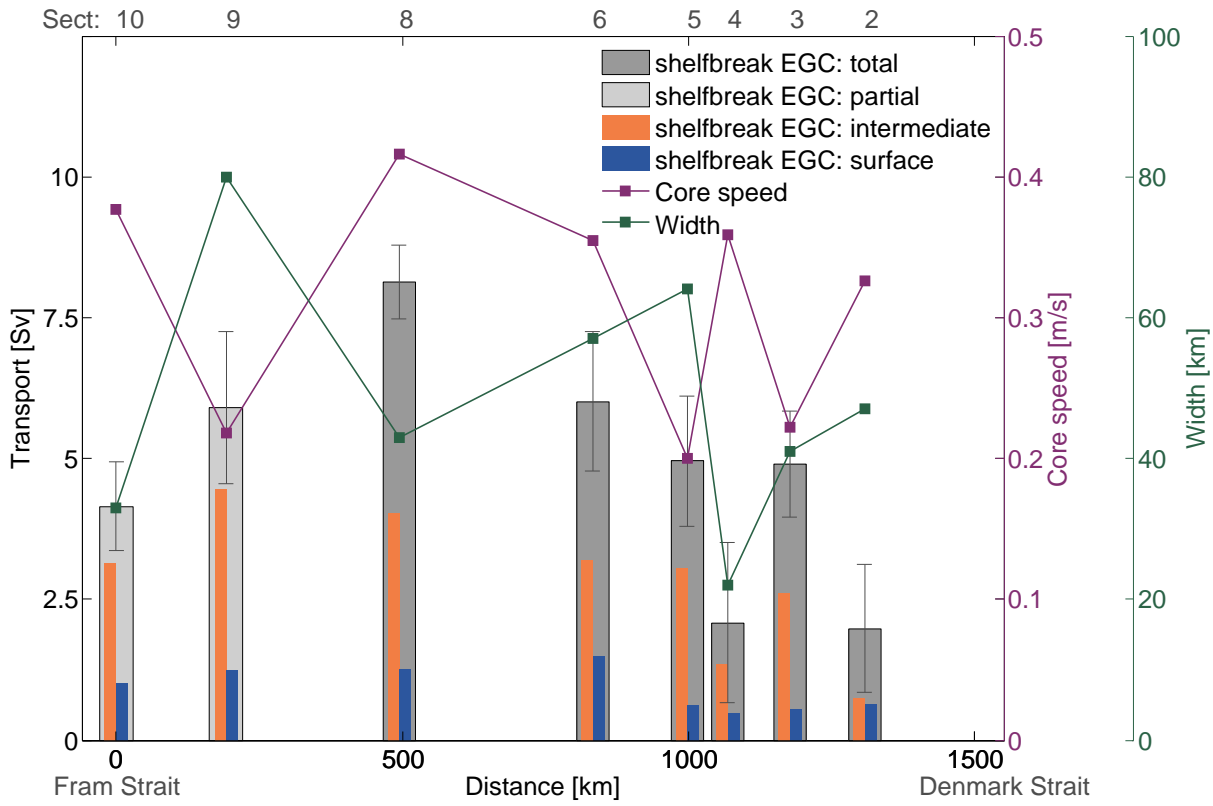


**Figure 6.** Volume transport of the shelfbreak EGC at each of the sections. The dark gray bars represent the volume transport where the entire branch was sampled and for sections 9 and 10 the light gray bars indicate that only the upper 800 m was measured. The orange and blue bars show the transport of intermediate and surface layers, respectively. Also shown are the core speed (purple line) and the width (green line) of the shelfbreak EGC. The x-axis indicates the along-stream distance from Fram Strait to Denmark Strait.

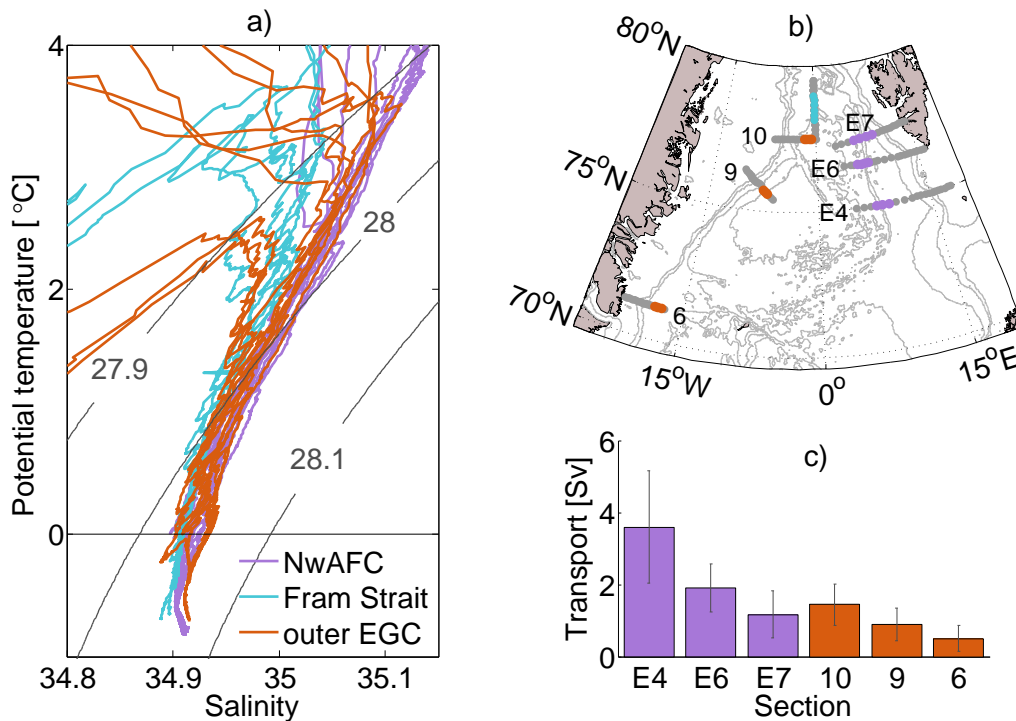


**Figure 7.** (a) Potential temperature/salinity diagram of the stations in the NwAFC/western branch of the WSC and the outer EGC, where the stations from the meridional section (named Fram Strait) are represented by the profiles from 2003. The three stations in orange with a temperature maximum just above 2 °C are from section 6. (b) map of the sections where these branches of the current system were detected, with the stations shown in panel (a) highlighted in colors. (c) transport of Atlantic-origin Water in this part of the current system, where positive transport is in the along-stream direction.

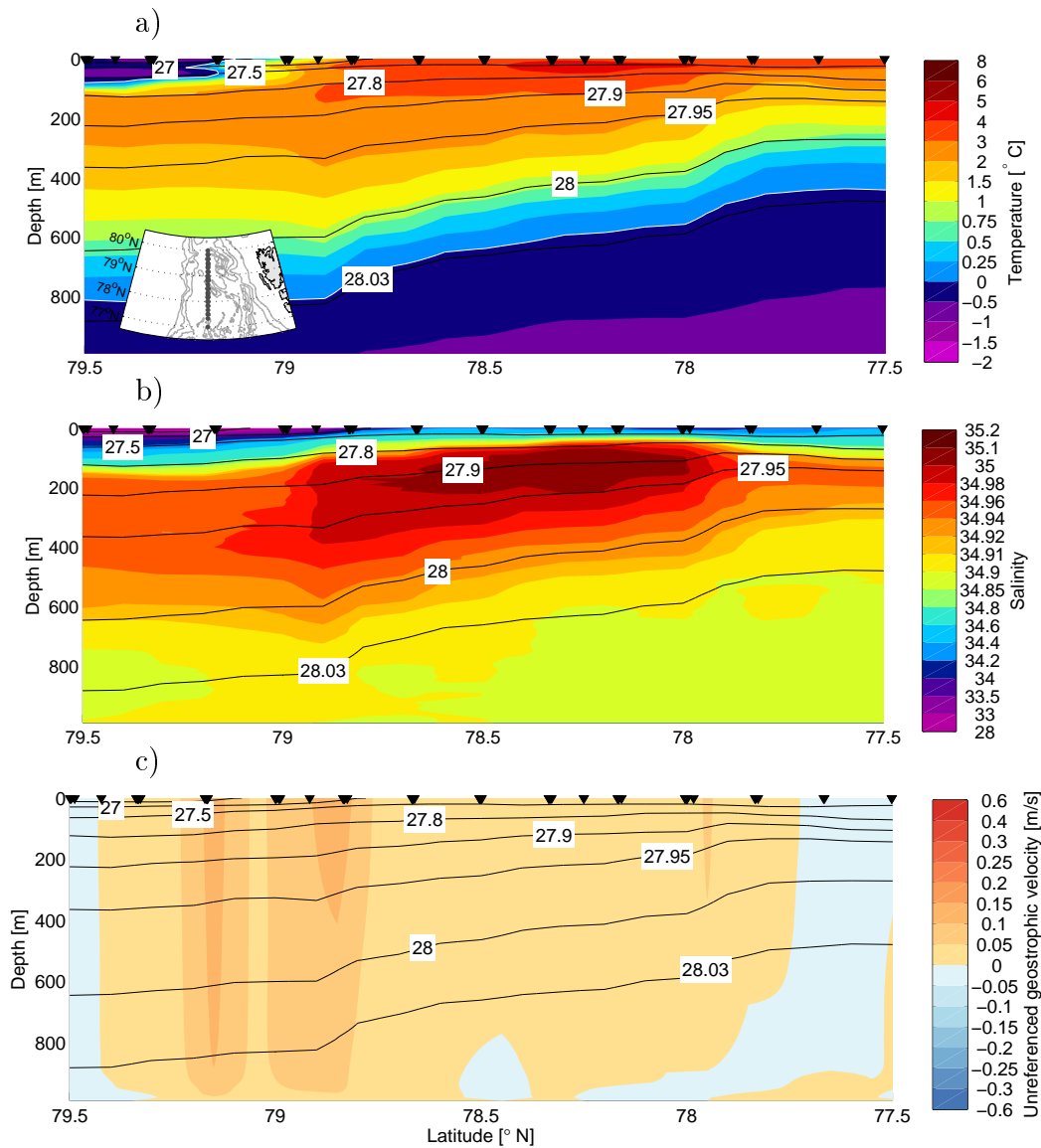


**Figure 8.** Mean meridional (close to 0°E) vertical section of (a) potential temperature, (b) salinity, and (c) geostrophic velocity relative to a level of no motion at 1000 m, based on Fram Strait summer sections from the years 1997, 1998, 1999, 2002, 2003, and 2004. The inset shows the location of the section. Positive flow is towards the west. The white contours in (a) are the 0 °C isotherm and the black contours are isopycnals ( $\text{kg}/\text{m}^3$ ). The black inverted triangles along the top indicate the locations of the 75 stations contributing to the mean.

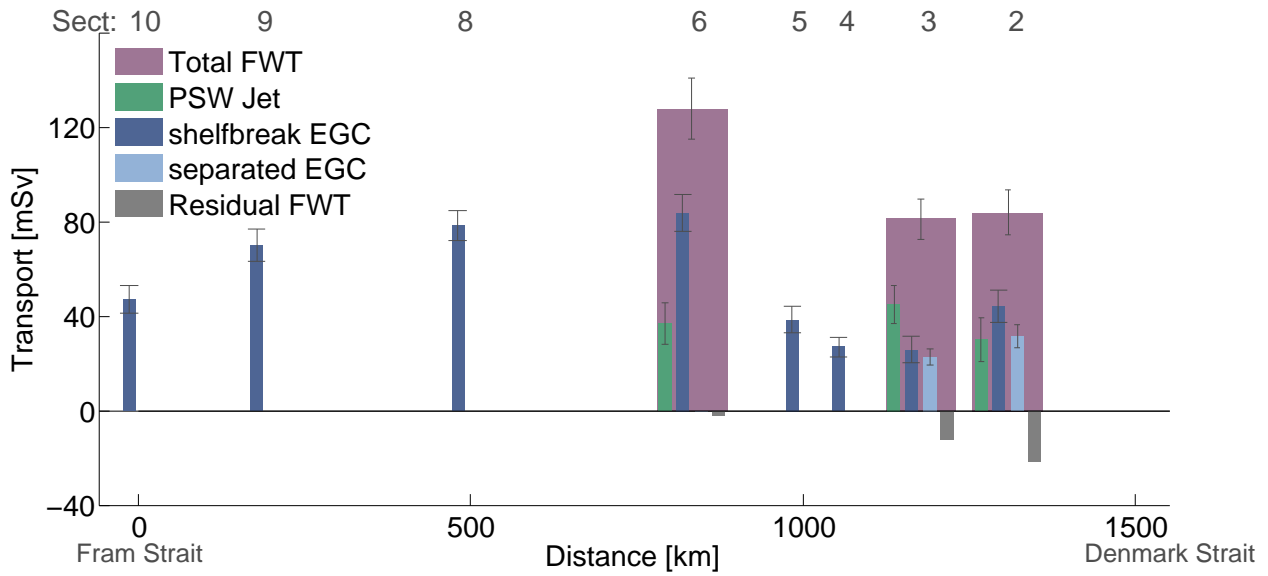


**Figure 9.** Freshwater transports in the different branches of the EGC system (PSW Jet in green, the shelfbreak EGC in dark blue, and the separated EGC in light blue), using a reference salinity of 34.8 (see Eq. 1). The purple bars show the total FWT for those sections covering the entire shelf. The residual transport (gray bars) is the transport outside the defined branches. The x-axis indicates the along-stream distance from Fram Strait to Denmark Strait.

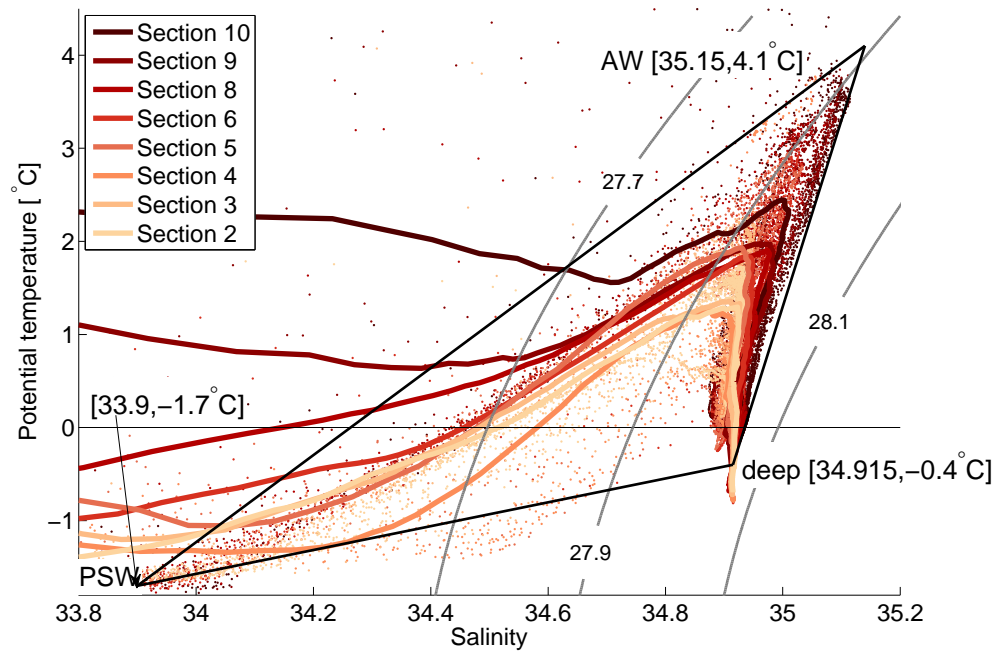


**Figure 10.** Potential temperature/salinity diagram of all profiles from the EGC survey where Atlantic-origin Water was present. The dots are individual measurements and the solid lines represent the mean profile from each section. The end members discussed in the text are indicated by the corners of the triangle. AW is Atlantic Water.

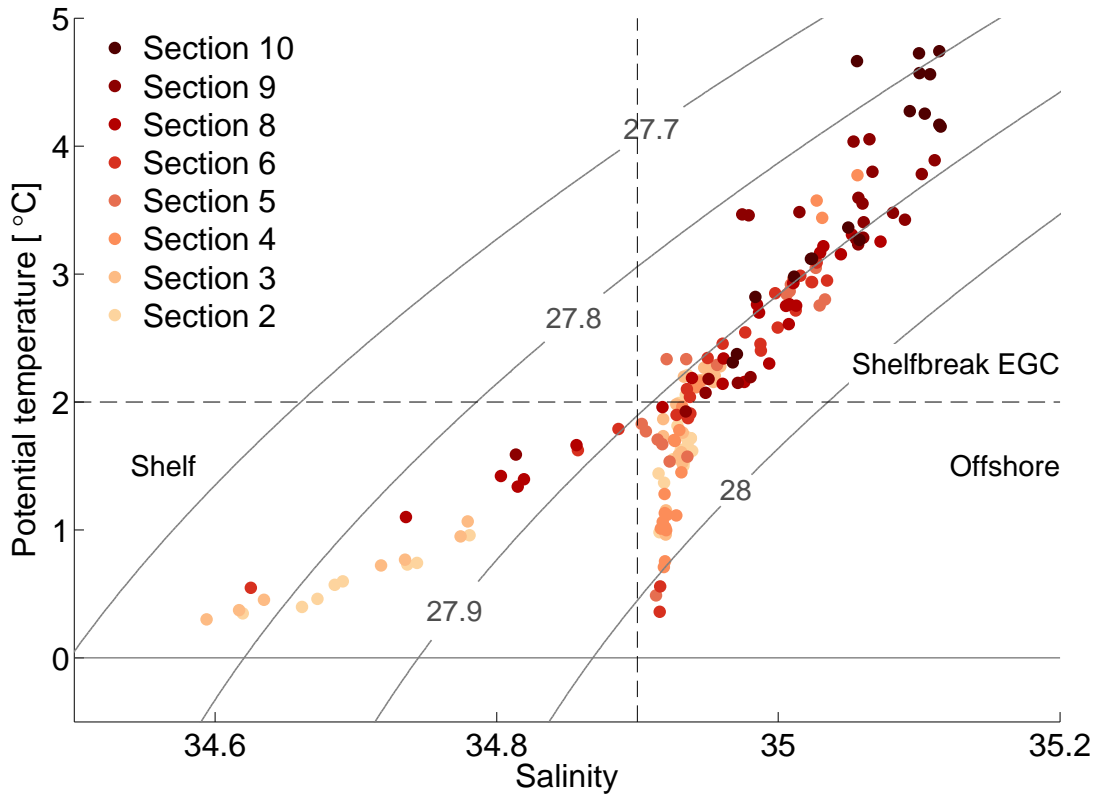


**Figure 11.** Potential temperature/salinity values corresponding to the core of the Atlantic-origin Water for the stations of the EGC survey. The horizontal dashed line is the 2 °C isotherm and the vertical dashed line is the 34.9 isohaline. The quadrants discussed in the text correspond to the shelfbreak EGC (also containing some offshore stations), the offshore water, and the water on the shelf.

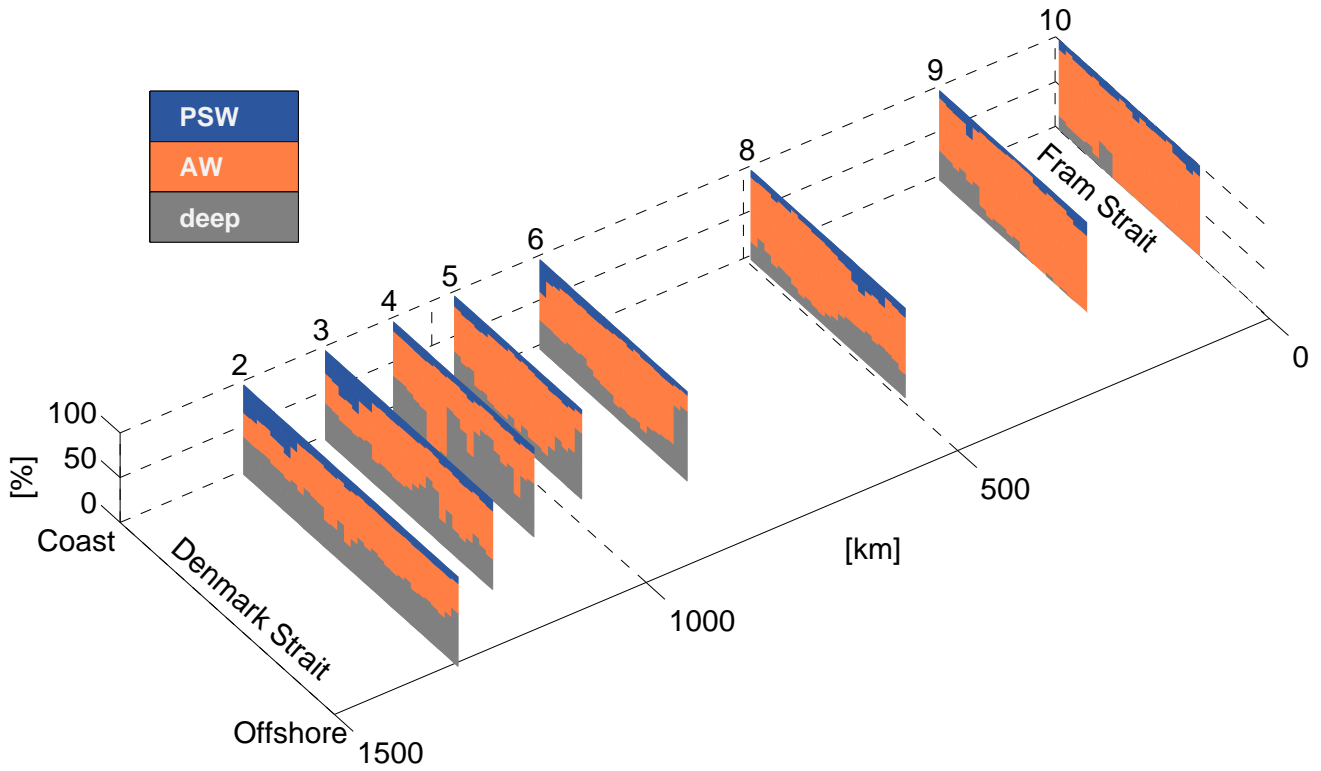


**Figure 12.** Percent contribution of the water mass end members in Fig. 10 to the core properties of the Atlantic-origin Water. The sections are labeled on top of the z-axis and plotted relative to their along-stream distance from Fram Strait.



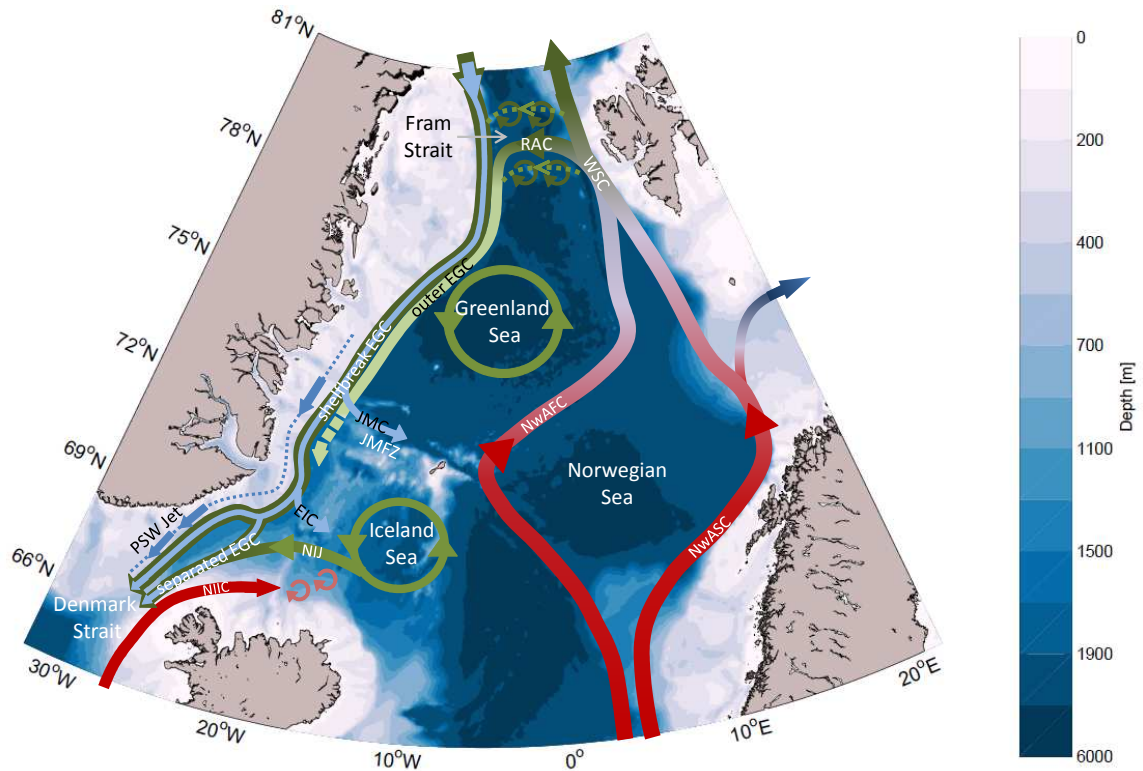


**Figure 13.** Schematic circulation in the Nordic Seas. The transformation of warm Atlantic Water to colder, fresher, and denser Atlantic-origin Water in the rim current of the Nordic Seas and Arctic Ocean is illustrated with a transition from red to green colors. The fresh PSW in the EGC is indicated in blue. The green circles in the Greenland and Iceland Seas indicate cyclonic gyres. The acronyms are: NwASC = Norwegian Atlantic Slope Current; NwAFC = Norwegian Atlantic Frontal Current; WSC = West Spitsbergen Current; RAC = Return Atlantic Current; JMC = Jan Mayen Current; JMFZ = Jan Mayen Fracture Zone; NIJ = North Icelandic Jet; EIC = East Icelandic Current; and NIIC = North Icelandic Irminger Current.